










Original Research

Strontium Changes Lipid Profile, Release, and Function of Matrix Vesicles Produced by Mineralization-Competent Cells

Larwsk Hayann^{1,2,*} , Mairobys Socorro² , Adriana Ferreira Lopes Vilela¹ ,
Juçara Gastaldi Cominal¹ , Luiz Henrique da Silva Andrilli¹ , Pietro Ciancaglini¹ ,
Saida Mebarek³ , Dobrawa Napierala² , Ana Paula Ramos¹ 

¹Department of Chemistry, Faculty of Philosophy, Sciences, and Letters, University of São Paulo, 140400-900 Ribeirão Preto, São Paulo, Brazil

²Department of Oral and Craniofacial Sciences, Center for Craniofacial Regeneration, University of Pittsburgh School of Dental Medicine, Pittsburgh, PA 15261, USA

³Institut de Chimie et Biochimie Moléculaires et Supramoléculaires, Université Lyon 1, UMR CNRS, 5246 Villeurbanne Cedex, France

*Correspondence: hayann.larwsk@gmail.com (Larwsk Hayann)

Academic Editors: Enrico Ragni and Graham Pawelec

Submitted: 24 October 2025 Revised: 21 November 2025 Accepted: 2 December 2025 Published: 23 December 2025

Abstract

Background: Mineral deposition in the extracellular matrix (ECM) is a highly organized process initiated by matrix vesicles (MVs) released from mineralization-competent cells, such as osteoblasts. In bone pathologies, osteogenic inducers (ions, hormones, nanoparticles) are becoming increasingly vital for the repair of damaged tissue. Among these inducers, strontium ranelate (SR), first suggested for treating osteoporotic patients, stands out. The bioactive strontium ion (Sr^{2+}) has a dual mechanism of action in bone homeostasis: it activates osteoblasts, promoting bone formation, and inhibits osteoclasts, limiting bone resorption. Recent research has focused on how Sr^{2+} influences osteoblast function, but its effects on the mineralization process have not been explored. For this study, we hypothesized that Sr^{2+} modulates mineralization-competent cells at two levels: (a) it activates the extracellular signal-regulated kinase 1/2 (Erk1/2) and cAMP response element-binding protein (CREB) osteogenic signaling pathways, increasing mineral towards in the ECM, and (b) it regulates MV release and function. Advanced lipidomic analysis examined how Sr^{2+} affects the MV lipid profile, which is pivotal for MV biogenesis and bone formation. **Methods:** We performed an MTT assay to assess the cytotoxicity of CaCl_2 and SR. Alizarin Red and Von Kossa staining were used to track mineral deposition towards the ECM. We assessed the phosphorylation states of ERK and CREB by western blotting and the osteogenic-related gene levels by quantitative real-time PCR. Biophysical characterization of 17A11-derived MVs was performed by nanoparticle tracking analysis (NTA), dynamic light scattering (DLS), and zeta potential. Mineral deposition and characterization were performed by turbidimetry and Fourier transform infrared spectroscopy (FTIR), respectively. MV activity was studied by alkaline phosphatase activity. We also performed a Western blot analysis to assess MV markers. Atomic force microscopy (AFM) and transmission electron microscopy (TEM) were applied to investigate changes in membrane fluidity and the vesicles' conformation. We explored the changes in lipid profiles using state-of-the-art lipidomic analysis. **Results:** Our findings demonstrate that Sr^{2+} activates the Erk1/2 and CREB pathways, leading to a dose-dependent increase in ECM mineralization. Additionally, the viscoelastic properties of MVs from Sr^{2+} -stimulated 17A11 cells, a *preodontoblast progenitor cell line*, were altered, as demonstrated by AFM and TEM, which we linked to modifications in their lipid composition, as revealed by the enrichment of ceramide (Cer) and sphingomyelin (SM), both of which play pivotal roles in bone development. **Conclusions:** Our study demonstrated that Sr^{2+} affects the initiation of the mineralization process by changing the release and lipid composition of MVs, and acts, in part, through Erk1/2 and CREB signaling pathways.

Keywords: strontium ranelate; biomineralization; extracellular vesicles; matrix vesicles; lipidomics

1. Introduction

Mineral deposition within the extracellular matrix (ECM) is a tightly regulated event that occurs during the formation of bone, hypertrophic cartilage, and mineralized dental tissues such as enamel, dentin, and cementum. A key component in initiating this process is the release of matrix vesicles (MVs) from cells capable of promoting mineralization. These vesicles are small, membrane-bound particles—typically about 100–300 nm in diameter—that represent a specialized subtype of extracellular vesicles. Their distinctive role lies in their ability to concentrate Ca^{2+}

and inorganic phosphate ($\text{P}_i/\text{PO}_4^{3-}$), creating a microenvironment suitable for the first hydroxyapatite (HAP) crystals to form. After release, MVs interact with type I collagen fibrils in the ECM, where the newly formed HAP nuclei can expand and align into the organized mineral phase characteristic of skeletal and dental matrices. Through these combined actions, MVs serve as essential initiators of ECM mineralization [1].

Advanced high-resolution imaging techniques have clarified the cellular pathways that govern how mineralizing cells generate and secrete MVs [2–5]. Evidence indi-



cates that microvesicles enriched with mineral content are released from the plasma membranes of both skeletal cells and odontoblasts [6–9]. Thus, MV release probably occurs through a mechanism involving the apical membrane, called microvilli budding from the plasma membrane [1]. Comparative proteomic and lipidomic analyses have also identified that MVs and the parental cell membrane microvilli share similar molecular composition [10,11]. For example, lipidomic data have revealed that fatty acids (FA) found in microvilli membranes and chondrocyte-derived MVs are similar [10]. In addition, the MV membrane contains high levels of cholesterol, sphingomyelin (SM), and phosphatidylcholine, which are highly abundant in lipid rafts [12,13]. Lipid class and organization influence the MV mineralization activity, as shown previously [14–17].

For the first HAp seeds to nucleate inside the MV lumen, specialized enzymes and transporters must act to promote Ca^{2+} (uppercase) and P_i uptake [18,19]. Previous reports have demonstrated that Ca^{2+} and P_i effectively induce MV biogenesis [20–24]. Recent proteomic data have revealed that a P_i transporter (PiT-1) and a calcium transporter (Annexins A2) [11,25,26] are localized in the MV membrane. In addition, the MV membrane hosts three key enzymes responsible for producing inorganic phosphate: tissue-nonspecific alkaline phosphatase (TNAP/ALP) and nucleotide pyrophosphatase phosphodiesterase-1 (NPP1), both of which generate P_i through adenosine triphosphate (ATP) hydrolysis, and PHOSPHO1, which releases P_i by cleaving phospholipid head groups such as phosphoethanolamine [27–30]. More than supporting HAp nucleation and structural organization within the collagenous ECM, MVs exert functions related to mineralized tissue physiology, such as inducing osteogenic differentiation [31]. Under osteogenic conditions *in vitro*, MVs mineralize type I-collagen [32–35]. Furthermore, MVs embedded in collagen-based hydrogels accumulate Ca^{2+} in a dose-dependent manner [36]. Collectively, these findings suggest that MVs may serve as promising therapeutic agents for bone-related disorders [31,37–43].

MVs are capable of initiating mineral deposition within the ECM; however, the regulatory cues that control their release from mineralizing cells remain incompletely defined. Owing to the ability of Sr^{2+} to both stimulate osteoblast-driven mineral formation and suppress osteoclast-mediated bone resorption, strontium ranelate (SR) has been broadly used in clinical management of osteoporosis [44–47], and has been linked to reducing fractures in the femoral neck [44,48–50]. Enhanced mineralization by osteoblasts could be related to MV release, but how Sr^{2+} influences MV biogenesis and function has not been investigated in depth. Studies have demonstrated that Sr^{2+} interferes with signaling pathways in differentiating mesenchymal stem cells (MSCs) into osteoblasts and osteoblast activity [50]. For instance, Sr^{2+} can engage key osteoblast-related receptors, including Frizzled/Lrp5/6 and

the calcium-sensing receptor (CaSR), leading to increased expression of osteogenic genes such as runt-related transcription factor 2 (*Runx2*), osteocalcin (*Ocn*), bone morphogenetic protein 2 (*Bmp2*), collagen type I (*Col1*), and transcription factor osterix (*Sp7*) [51,52]. Previous studies have also demonstrated the “promiscuous” Sr^{2+} effect over other osteogenic-related signaling pathways, including the Erk1/2 [53], Bmp2 [54,55], Wnt/ β -catenin [56–58], and AMPK/mTOR signaling pathways [59,60], and others [61]. Interestingly, not much has been shown regarding the part played by Sr^{2+} in activating the transcription factor cyclic AMP response-binding protein (CREB) signaling pathway, even though this pathway is activated in bone physiology [62,63].

On the other hand, for monocyte/macrophage progenitor cells to differentiate into mature osteoclasts, nuclear factor-kappa beta ($\text{NF-}\kappa\beta$), which is activated by the receptor activator of $\text{NF-}\kappa\beta$ ligand (RANKL), must be regulated [64]. Similarly, Ca^{2+} induces Normal Bone Marrow Stromal Cells (NBMSC) differentiation into mature osteoclasts through CaSR activation, to promote $\text{NF-}\kappa\beta$ nuclear translocation. Curiously, CaSR activation by Sr^{2+} inhibits osteoclast maturation [44,65,66]. Therefore, different cellular responses emerge despite the similarities between Ca^{2+} and Sr^{2+} . Given that Sr^{2+} has versatile activity on osteoblasts and osteoclasts, numerous studies have been conducted about the use of strontium in different forms (e.g., soluble ion, linked to other organic and inorganic compounds, or associated with scaffolds) [67–73] aiming at bone regenerative medicine.

Although Sr^{2+} is often presumed to promote mineralization due to its chemical similarity to Ca^{2+} , the detailed cellular pathways and molecular mechanisms through which Sr^{2+} influences biomineralization are still poorly defined. We proposed that Sr^{2+} contributes to biomineralization through two complementary mechanisms: (a) by promoting the differentiation and activation of cells capable of initiating mineralization, and (b) by enhancing both the release and functional activity of MVs. To investigate the first mechanism, we examined the involvement of the Erk1/2 and CREB signaling pathways and assessed changes in osteogenic gene expression using qRT-PCR. We also evaluated how Sr^{2+} modulates MV secretion and their subsequent mineralizing capacity. Lastly, we characterized, for the first time, the effects of Sr^{2+} on the MV lipidomic profile, demonstrating how shifts in lipid composition influence the vesicles’ ability to drive ECM mineralization.

2. Materials and Methods

2.1 Cell Culture Conditions and Treatment

Mouse preodontoblast-derived 17IIA11 cells were kindly provided by Prof. Dr. Odile Kellermann and Prof. Dr. Anne Poliard, *Laboratoire de Différenciation Cellulaire et Prions-UPR, France*. The preodontoblast isolation method and characterization are described elsewhere

[74,75]. Mycoplasma testing was performed by PCR, and all tests yield negative results. Standard flow cytometry technique were used to validate the cell surface epitope profile of the pulpal 17IIA11 clones. Cells were maintained in a “growth medium” consisting of Dulbecco’s modified Eagle’s medium (DMEM; Gibco, Thermo Fisher Scientific, Logan, UT, USA), enriched with 5% (v/v) fetal bovine serum and 1% (v/v) penicillin/streptomycin. Incubation was carried out at 37 °C in a humidified chamber with 5% CO₂ and 95% air. For differentiation experiments, cells were seeded into 10-cm dishes at a density of 2×10^6 cells. Once the cultures reached confluence, osteogenesis was induced using an “osteogenic medium”. This medium was prepared by supplementing the basal formulation with 50 µg/mL ascorbic acid (AA) and 5 mM sodium phosphate buffer (NaH₂PO₄/Na₂HPO₄, pH 7.4).

2.2 Cell Viability Analysis—MTT Assay

The cells were cultured for 24 h or 4 or 6 days, and cell viability was assessed by the MTT 3-(4,5-dimethylthiazol-2-yl)-2,5-diphenyltetrazolium bromide assay as previously described here [76]. To measure the metabolic activity, the generated formazan product was solubilized in DMSO, and the optical density was recorded at 570 nm.

2.3 Alizarin Red Staining Assay

Cells (1×10^6) were inoculated into 12-well plates and stimulated for 4 to 6 days with 5 mM Pi, SR (0.1–1.0 mM), or CaCl₂ (0.1–1.0 mM). Post-treatment, fixation was performed with 4% paraformaldehyde. Mineral deposition was stained using 40 mM Alizarin Red-S (Sigma) for 10 minutes, after which the wells were washed with deionized water to eliminate excess stain.

2.4 Von Kossa Staining Assay

The staining process began with two washes in PBS and fixation using 4% paraformaldehyde for 10 min. After rinsing twice with deionized water, the cells were incubated with a 2% silver nitrate solution. The formation of the silver precipitate required 20 min of UV lamp exposure, followed by a water rinse. The reaction was subsequently stopped by adding 5% sodium thiosulfate for 5 min, finalized by a deionized water wash.

2.5 Quantitative RT-PCR

Total RNA was isolated using the Trizol protocol (0000124780; Invitrogen, Thermo Fisher Scientific, Waltham, MA, USA) and purified with the GenElute Mammalian Total RNA miniprep kit (Sigma). 1 µg of RNA was subjected to DNase I (Invitrogen) treatment and reverse-transcribed into cDNA using the SuperScript III kit (Invitrogen). Gene expression was quantified by real-time PCR on an AB Biosystems 7500 system employing the Fast SYBR Green reaction mix (4385618; Roche Applied Science, Penzberg, Bavaria, Germany). Primer sequences

were as follows: *Osx* F, GGGCGTTCTACCTGCGACTG, and R, ATCGGGGCGGCTGATTG; *Runx2* F, TGGC-CGGAATGATGAGAAAC, and R, TGAAACTCTTGC-CTCGTCCG; *Phospho1* F, CCTGGGAAACAGCCGC-CGATGTG, and R, CCCGGAGGAGCATAGCAAAGC-GAAG; *Gapdh* F, GCAAGAGAGGCCCTATCCCAA, and R, CTCCCTAGGCCCTCCTGTTATT; *Colla1* F, GCAACAGTCGCTTCACCTACA, and R, CAAT-GTCCAAGGGAGCCACAT; *Alpl* F, CAGTGGGAGT-GAGCGCAGCC, and R, GCACTGGGTGTGGCGTG-GTT; *Smpd3* F, ACATCGATTCTCCACCAACACCT, and R, AATTCGCACAATGCAGCTGTCCTC.

2.6 Western Blot Analysis

For immunoblotting experiments, cells were seeded in six-well plates at a density of 5×10^5 cells per well. After a 24-h attachment period, the basal culture medium was replaced with either basal medium containing 5 mM Na-Pi, osteogenic medium supplemented with SR (0.1–1.0 mM), or osteogenic medium containing CaCl₂ within the same concentration range. Protein lysates were obtained by harvesting the cells in RIPA buffer enriched with phosphatase and protease inhibitor reagents (1 mM NaF, 2 mM Na₂VO₄, 2 mM leupeptin, 2 mM pepstatin, 2 mM PMSF, and 10 µM MG132). Protein levels were first quantified using a micro-BCA assay kit (Thermo Scientific, Rockford, IL), followed by confirmation with the Bradford method (1976) using BSA (0.1 mg/mL) as a calibration standard. Equal amounts of protein (15 µg per sample) were resolved on 4–12% Bis-Tris precast gels (Invitrogen) and transferred to nitrocellulose membranes. Target proteins were visualized using the Odyssey Infrared Imaging System (LI-COR Biosciences, Lincoln, NE, USA). The following primary antibodies were applied at the indicated dilutions: phospho-Erk1/2 (1:2000), total Erk1/2 (1:1000), phospho-CREB (1:2000), total CREB (1:1000) (all from Cell Signaling), tissue-nonspecific alkaline phosphatase (1:1000, R&D Systems), annexin V (1:2000, Abcam), α -tubulin (1:10,000, Sigma), and Lamp2a (1:1000, Abcam). Fluorescent secondary antibodies from LI-COR were used at 1:20,000 for detection.

2.7 Matrix Vesicle Isolation and Purification

MVs were isolated and purified from the ECM as described previously [16,77]. Cells were washed with PBS, and MVs were released by digesting the ECM with 2.5 mg/mL collagenase IA (102764679; Sigma-Aldrich, St. Louis, MO, USA) and 2 mM CaCl₂ for 4 h at 37 °C in 5% CO₂. The digestion mixture was collected and centrifuged at 600 \times g for 20 min to remove cells. The supernatant was then spun at 20,000 \times g for 30 min to clear debris and at 30,000 \times g for 60 min to pellet MVs. The pellet was washed once in Tris-buffered saline TBS, centrifuged again at 30,000 \times g for 60 min, and finally resuspended in 150 µL TBS before storage at –80 °C.

2.8 Nanoparticle Tracking Analysis (NTA)

MV size and concentration were measured by NTA using a NanoSight NS300 (Malvern Instruments Ltd., Worcestershire, UK). Samples were diluted in filtered PBS (pH 7.4) to reach the recommended range of 1×10^8 – 1×10^9 particles/mL. Measurements were collected and processed with NTA 2.3 Analytical Software (Malvern, Worcestershire, UK). For each sample, five 60-s videos were acquired at camera level 10 while the suspension was kept at room temperature under continuous syringe pump flow. A detection threshold of 10 was applied for analysis. The number of MVs released per cell was calculated by dividing the total particle count by the corresponding cell number [78].

2.9 Transmission Electron Microscopy (TEM)

MV morphology and size were examined by JEOL JEM-100 CXII (JEOL Ltd., Akishima, Tokyo, Japan) TEM by drying a drop of the MV colloidal dispersion on a copper grid covered with a conductive polymer. Then, the sample was treated with phosphotungstic acid (PTA, 1%) for 15 min and analyzed.

2.10 Atomic Force Microscopy

MVs were passed through 0.22- μ m Millipore® filters to remove aggregates and residual matrix fragments. To preserve vesicle structure, samples were fixed with 1.4% glutaraldehyde and incubated at 37 °C for 5 min. A 15- μ L aliquot of each preparation was then placed on freshly cleaved mica, air-dried, and imaged using a SPM-9600 (Shimadzu Corporation, Kyoto, Japan) scanning probe microscope.

2.11 Mineral Analysis by ATR-FTIR

Mineral composition was assessed by ATR-FTIR using an IRPrestige-21 spectrometer (Shimadzu Corporation, Tokyo, Japan). Mineral deposits formed in the presence of MVs were gently collected from the culture plate and positioned on a ZnSe ATR crystal for analysis [13,79].

2.12 Tissue Nonspecific Alkaline Phosphatase Activity

TNAP activity was determined according to Andrilli *et al.* (2023) [28]. TNAP activity was quantified by monitoring the formation of the p-nitrophenyl product generated from p-nitrophenylphosphate (pNPP) at pH 10.4. Absorbance was recorded at 405 nm. Enzyme activity was expressed as U per mg of total protein, where one unit corresponds to the hydrolysis of 1 nmol of substrate per mg of protein at 37 °C.

2.13 Matrix Vesicle In Vitro Mineralization—Turbidimetry

MVs were first incubated in synthetic cartilage lymph (SCL) buffer (pH 7.5) containing 2 mM Ca^{2+} , 2 mM Mg^{2+} , 16.5 mM Tris, 63.5 mM sucrose, 5.55 mM glucose, and the indicated concentrations of Na^+ , K^+ , Cl^- , HCO_3^- ,

and SO_4^{2-} . ATP (2 mM) served as the phosphate source. Mineral formation was monitored by measuring turbidity at 340 nm using a SpectraMax® M3 microplate reader. Each value was corrected by subtracting the initial absorbance of the corresponding MV sample [28,80].

2.14 Statistical Analysis

All the experiments were conducted at least three times. Data are presented as the mean \pm SD. The ANOVA test was applied for statistical analysis. Values were considered significant when $p < 0.05$ (*).

2.15 Untargeted Lipidomic Analysis

2.15.1 Standard Solutions

Synthetic lipid standards were acquired by Avanti Polar Lipids (Alabaster, Alabama, USA) and used as internal lipids standards such as: monoacylglycerophosphocholine (LPC) 17:0, monoacylglycerophosphate (LPA) 17:0, diacylglycerophosphocholine (PC) 17:0/17:0, phosphatidylserine (PS) 17:0/17:0, diacylglycerophosphoethanolamine (PE) 17:0/17:0, diacylglycerophosphoglycerol (PG) 17:0/17:0, SM 12:0 and ceramide (Cer) 17:0. Stock solutions of each synthetic IS were prepared by dissolving in $\text{CHCl}_3/\text{MeOH}$ (9:1 or 5:1, v/v) at concentrations ranging from 25 mM to 5 mM and stored at -80 °C. Working solutions were prepared at 25 μ M for the assays.

2.15.2 Sample Preparation

Extraction of samples was carried out based liquid-liquid phase extraction protocol as described here [81]. Briefly, each sample was spiked with 40 μ L of a mixture of lipid (IS) before being extracted. MV (100 μ L - 10^{11} particles) samples in Eppendorf tubes were adjusted in volume with deionized ultrapure water to 250 μ L and mixed with 260 μ L MeOH. Followed by the addition of 1000 μ L MTBE and vortexed for 10 s. The tubes were incubated in an ice bath for 10 min and followed put on a shaker for 60 min, under gentle stirring at room temperature. Afterwards, the extraction solution was centrifuged at 12,000 g for 10 min, followed by the collection of the upper organic phase. At the end of extractions, all collected samples were dried in a vacuum system at a pressure of 10.0 Torr at 45 °C. The dried samples were re-suspended in 40 μ L isopropanol/acetonitrile/ H_2O (2:1:1 v/v/v) and analyzed by an LC-MS/MS system.

2.15.3 LC-MS/MS Conditions Tandem Mass Spectrometry Analysis

Tandem mass spectrometry analyses were carried out in an ultra-high-performance liquid chromatographic (UHPLC - Nexera X2; Shimadzu, Kyoto, Honshu, Japan) coupled to a triple quadrupole time-of-flight (Triple- TOF® 5600+ Sciex, Foster, CA, USA) mass spectrometer. The UHPLC system consists of two LC 30AD pumps, an au-

tosampler (SIL-30AC), a CTO-30A oven, a CBM-20A controller, and DGU-20A degassing. The TripleTOF® 5600+ mass spectrometer was equipped with a turbo-V IonSpray and calibrant delivery system (CDS). Data acquisition was accomplished on a Shimadzu CBM-20A system interfaced with a computer, using the Analyst® TF software version 1.7.1 (SCIEX, CA, USA). The chromatographic separation was performed using an Acquity UPLC® CSH™ C18 column (100 × 2.1 mm; 1.7 µm) from Waters (Milford, USA). The mobile phases used were: phase A (0.1% formic acid and 10 mM of ammonium formate in water with acetonitrile—39.9:60 v/v) and phase B (0.1% formic acid and 10 mM of ammonium formate in isopropanol with acetonitrile—89.9:10 v/v). The column oven was set at 45 °C. The injection volume for each analysis was 5 µL, and the flow rate was set at 0.4 mL/min. Separations were made with a gradient as follows: 0.01–3 min, 30% B; 3.1–5.1 min, 43% B; 5.21–15.21 min, 65% B; 15.22–21.22 min, 85% B; 21.23–23.5 min, 100% B. Mass spectra were acquired from mass to charge ratio (m/z) 50 to 1250. The electrospray ionization (ESI) source operated in positive and negative modes. The parameters used for the mass spectrometer were: nebulizer gas (GS1) at 50 psi, turbo gas (GS2) at 60 psi, curtain gas (CUR) at 25 psi, electrospray voltage (ISVF) at +4500 V and –4500 V, and turbo ion spray source temperature at 500 °C. The dwell time was set at 10 ms, and a mass resolution of 35,000 was achieved at m/z 400.

External calibrations of the calibrated delivery system (CDS) were performed using an atmospheric pressure chemical ionization (APCI) probe. Automatic mass calibration (accuracy <1 ppm) was carried out after each of the five sample injections using the APCI Positive and Negative Calibration Solution (SCIEX, CA, USA), which was introduced by direct infusion at a flow rate of 350 µL/min.

2.16 Lipidomic Data Processing and Statistical Analyses

All datasets acquired were analyzed using the software PeakView 2.1 (Sciex, CA, USA) and MS-Dial™ 5.1.230429 (open-source software - RIKEN, Yokohama, Kanagawa, Japan). The setting parameters used were described here [81]. Briefly, the data were processed using SWATH acquisition files with centroid MS/MS data in both ionization modes. Parameters included an m/z tolerance of 0.05 Da, mass range of 50–1250, and specific settings for peak detection, deconvolution, and alignment. Lipid annotation was performed using the MS-DIAL software with the MSP 20230427074147 conventional as a reference library under defined mass accuracy and matching criteria. Identified lipid structures were confirmed by MS/MS fragmentation matching. The final dataset was exported in .svg or .xls formats for statistical analysis, which was conducted in GraphPad Prism 8.0 (San Diego, CA, USA) and MetaboAnalyst 6.0 (Xia Lab, McGill University, Montréal, Québec, Canada) using PLS-DA and heatmap visualization, with re-

sults expressed as mean ± SEM and significance set at $p < 0.05$.

3. Results and Discussion

3.1 Sr^{2+} Induces Biomineralization In Vitro

For our investigation into Sr^{2+} -mediated biomineralization, we used the 17IIA11 preodontoblast cell line, which offers a robust and relatively simple system for analyzing the contribution of MVs to dental tissue formation [78,82–84]. Additionally, 17IIA11 cells express high levels of major osteogenic transcription factors Sp7 and Runx2, so these cells are already committed to mineralization, mineralizing the ECM in approximately 6 days. Contrarily, MC3T3-E1, a pre-osteoblast cell line, fully mineralizes the ECM within approximately 21 days, making it a more scalable but also more time-consuming model.

However, despite their similarities, caution is warranted when extrapolating the findings presented here to bone tissue, as important differences between cell types are reported. For example, our group has observed a significant change in the protein and lipid profile of MVs derived from different mineralizing cell lines (data submitted for publication), which suggests a different mechanism of action and biogenesis. Therefore, we encourage further studies using primary osteoblasts or the MC3T3-E1 cell line to determine whether the effects of Sr^{2+} are consistent across different mineralizing cell types.

We used SR as the primary Sr^{2+} source because it has been used as a treatment to prevent fractures in postmenopausal osteoporosis [85–87]. SR is composed of an organic moiety (ranelic acid) and two atoms of stable strontium. One may raise the concern of the ranelic acid having any sort of organic anion effect. However, pharmacokinetics and metabolism investigation of the commercially available SR PROTOS® (CAS number: 135459-87-9) showed no evidence of ranelic acid accumulation and metabolism in animals and humans. Absorbed ranelic acid is rapidly eliminated unchanged via the kidneys [88]. Other works have also tested its reliability [87,89].

First, we tested the effect of Sr^{2+} on cell viability (Fig. 1a–f). We tested low (0.1 mM) and high (1.0 mM) concentrations of SR in osteogenic medium consisting of standard growth medium supplemented with AA and sodium phosphate (Na_3PO_4), so that the effect of Sr^{2+} with osteogenic inducers could be evaluated. Because Ca^{2+} is important for mineralization, and Sr^{2+} may have similar modes of action to Ca^{2+} [90,91], we also compared the effects of Sr^{2+} to the effects of Ca^{2+} . Fig. 1 shows that adding Sr^{2+} to osteogenic medium was not cytotoxic to 17IIA11 cells at any of the tested concentrations (see Fig. 1e,f).

We examined mineral deposition by Alizarin Red S and Von Kossa staining (Fig. 2). Given that alizarin red (Fig. 2, left column) stains Ca^{2+} -rich mineral nodules, and because we used Ca^{2+} in some assays, we performed Von

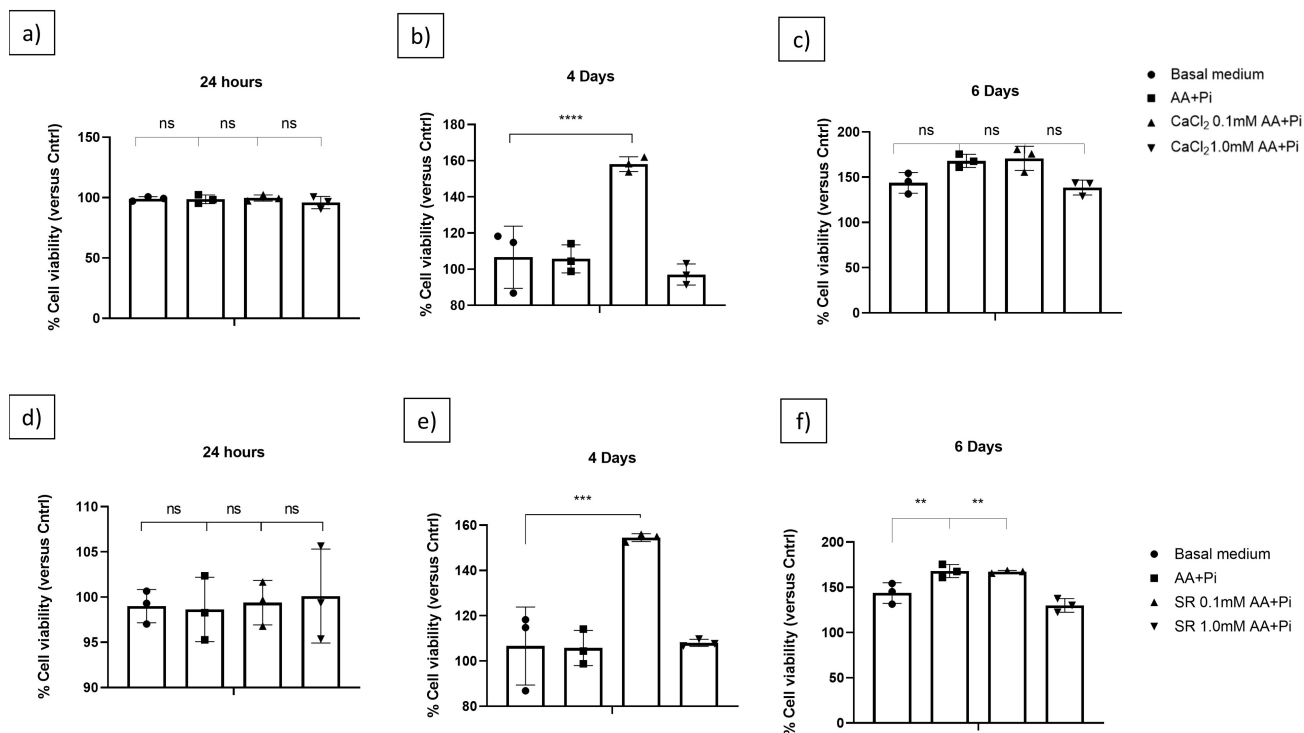


Fig. 1. Effect of osteogenic medium (AA+P_i) containing Ca²⁺ or Sr²⁺ on preodontoblast-derived 17IIA11 cell viability as compared to osteogenic medium alone. (a–c): cytotoxic effect of basal medium, AA + P_i, CaCl₂ 0.1–1.0mM after 24 h, 4, and 6 days of treatment. (d–f): cytotoxic effect of basal medium, AA+ P_i, SR 0.1–1.0mM after 24 h, 4, and 6 days of treatment. Neither Ca²⁺, as CaCl₂, nor Sr²⁺, as SR, exerts cytotoxic effects, irrespective of their concentration (0.1 or 1.0 mM) or culture time (24 h, or 4 or 6 days). One-way ANOVA was performed for multiple statistical comparisons. *p* values for CaCl₂ *****p* < 0.0001 and for SR ***p* < 0.005, ****p* < 0.0001. AA, ascorbic acid; SR, strontium ranelate; ns, not significant.

Kossa staining (Fig. 2, right column), a more precise histological technique when studying mineral deposition [92], to avoid false positives and to double-check mineral deposition. Von Kossa staining confirmed that 1.0 mM Sr²⁺ in osteogenic medium inhibited mineralization. Alizarin Red S and Von Kossa staining demonstrate accumulation of Ca and Pi, respectively, in the ECM after mineralization had been stimulated for four or six days. In a basal medium, Ca²⁺ (as CaCl₂) or Sr²⁺ (as SR) alone did not induce mineralization (Supplementary Fig. 1), which was expected given that AA has been reported to participate in the collagen synthesis cascade and that P_i is required for HAp formation. Under osteogenic conditions, Ca²⁺ and 0.1 mM Sr²⁺ did not affect mineralization (Fig. 2). In contrast, 1.0 mM Sr²⁺ in osteogenic medium inhibited mineralization, contradicting previous reports [93,94]. Because high Sr²⁺ concentrations in osteoblasts stimulate mineralization [95,96], whether impaired mineralization is dose-dependent or whether mineral deposition depends on the cell line [94] remains to be investigated.

3.2 Sr²⁺ Affects the Erk1/2 and CREB Signaling

The initiation of mineral deposition within the ECM is contingent upon cellular responses triggered by extracel-

lular signals [97–100]. This response involves transmitting the signal from the cell membrane through an intracellular signaling cascade, ultimately resulting in a change in the gene expression program. The molecular response of mineralization-competent cells varies depending on the stimulus, but the outcome is the increased expression of genes involved in biomineralization. Studies have shown that stimulation of cells with P_i activates Erk1/2 kinases, while stimulation with Ca²⁺ activates the CREB pathway [53,101]. Therefore, we investigated whether the effect of Sr²⁺ on mineralization is mediated by these molecules in 17IIA11 cells (Fig. 3). We analyzed the levels of active CREB (pCREB) and pErk1/2 after stimulating 17IIA11 cells for 15 and 30 min to verify early and late responses, respectively.

Western blot results revealed that activation of Erk1/2 and CREB in 17IIA11 cells varied according to both the duration of stimulation and the concentration of Ca²⁺ or Sr²⁺. Erk1/2 is activated in two stages, namely the first and second waves (after approximately 15 min and 8 h, respectively). However, this time varies depending on cell type [102,103]. In our system, these waves occurred at approximately 15 and 30 minutes, respectively (Fig. 3). During the early phase, Erk1/2 phosphorylation increased after

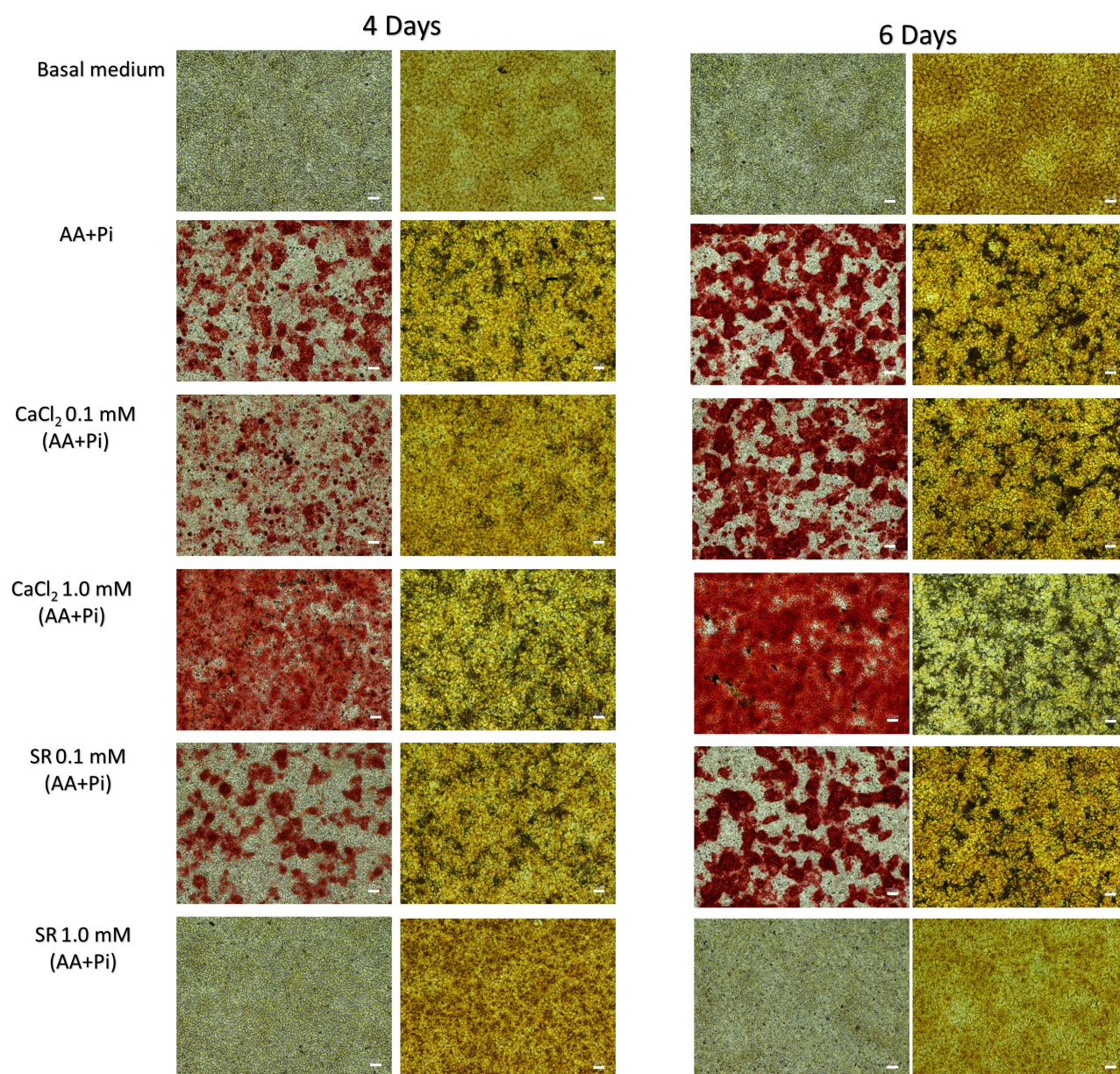


Fig. 2. Ca^{2+} (as CaCl_2) at 0.1 or 1.0 mM in osteogenic medium (AA+Pi), and Sr^{2+} (as SR) at 0.1 mM in osteogenic medium, support the mineralizing capacity of preodontoblast-derived 17IIA11 cells. In contrast, 1.0 mM Sr^{2+} in osteogenic medium impairs mineralization. Mineral deposition was evaluated using alizarin red S and von Kossa staining after four and six days of stimulation. The left and right columns show alizarin red S and von Kossa staining, respectively. All conditions were compared with osteogenic medium alone. Scale bar = 100 μm .

exposure to 0.1 mM Ca^{2+} or to 0.1- or 1.0-mM Sr^{2+} , suggesting that both ions can initiate early Erk1/2 activation, potentially in synergy with AA and Pi. However, clear differences emerged in the late response. Sr^{2+} at 0.1 mM continued to enhance Erk1/2 phosphorylation during the late phase, whereas Ca^{2+} did not. Thus, Sr^{2+} , but not Ca^{2+} , sensitized the Erk1/2 signaling pathway during prolonged stimulation.

CREB, a ubiquitous transcription factor involved in many cellular processes, is phosphorylated in response

to diverse stimuli, including growth factors, steroids, cytokines, and Ca^{2+} [104]. While dysregulated CREB activity is linked to cancer [105–107], CREB signaling also contributes to bone development and homeostasis [108,109]. In this study, 1.0 mM Sr^{2+} in osteogenic medium stimulated CREB phosphorylation during both early and late phases, whereas 1.0 mM Ca^{2+} induced CREB activation only during the early phase (Fig. 3). These findings mirror the behavior observed for Erk1/2, again indicating a broader temporal window of action for Sr^{2+} compared with

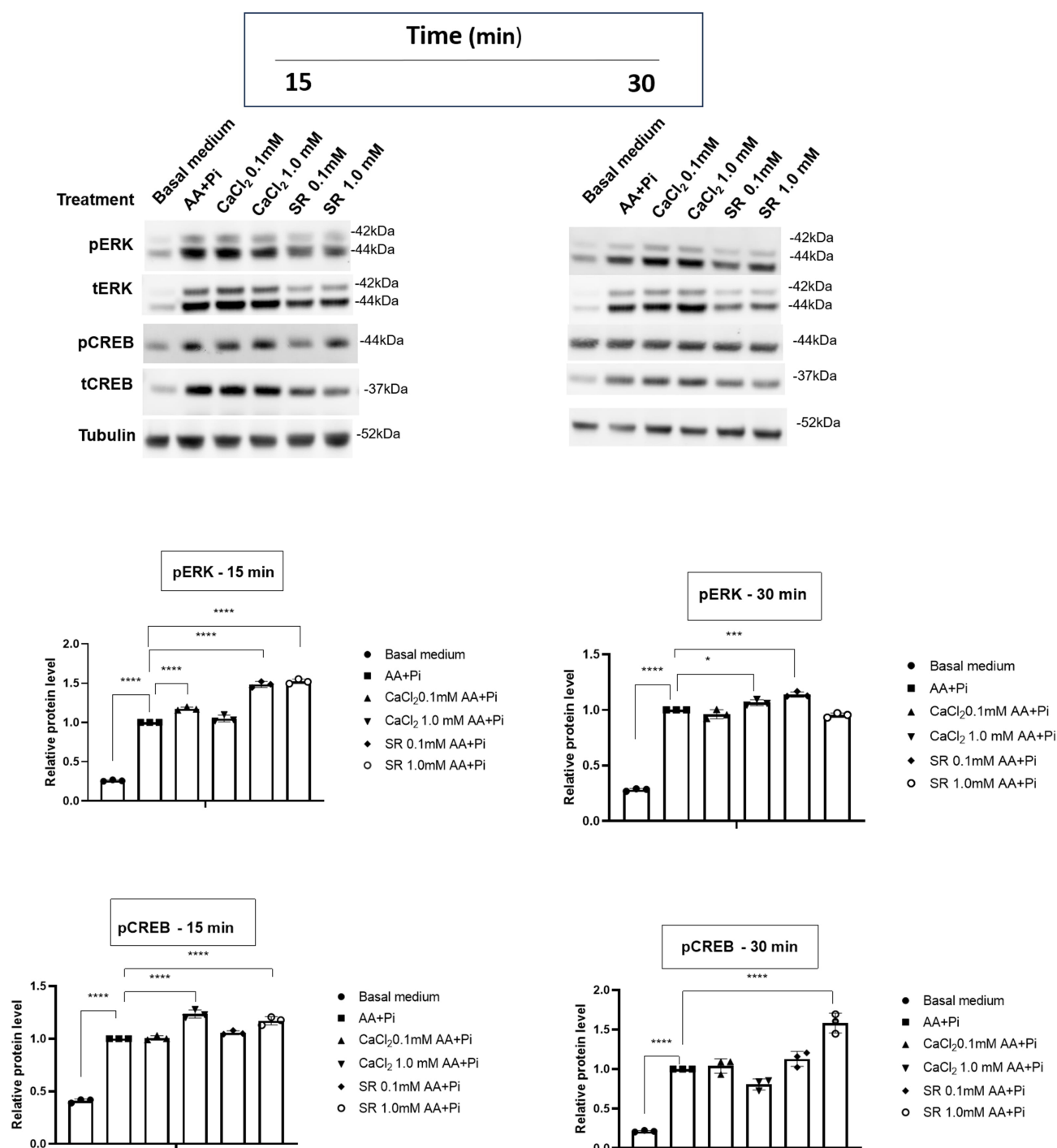
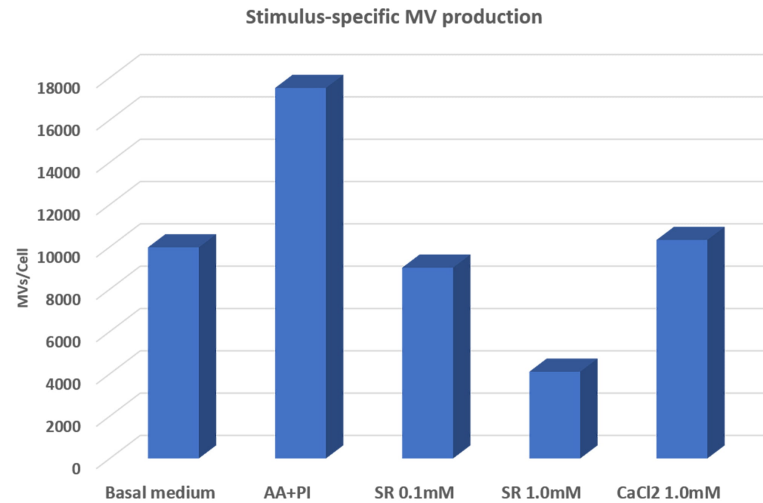


Fig. 3. Ca²⁺- or Sr²⁺-activated ERK1/2 and CREB signaling pathways in 17H1A11 cells. Activation of the ERK1/2 and CREB pathways was assessed by analyzing protein phosphorylation after stimulation with different concentrations of Ca²⁺ (as CaCl₂) or Sr²⁺ (as SR) in osteogenic medium (AA+Pi) for 15 or 30 minutes. All conditions were compared with osteogenic medium alone. Multiple statistical comparisons were performed by one-way ANOVA. *p* values for pERK 15 min *****p* < 0.0001 and 30 min **p* < 0.05, ****p* < 0.0001, and *****p* < 0.0001; *p* values for pCREB 15 min *****p* < 0.0001 and 30 min *****p* < 0.0001.

Ca²⁺. Because CREB and Erk1/2 activation are modulated by CaSR [110–112], which responds to both Ca²⁺ and Sr²⁺ [51] the differential activation profiles likely reflect distinct interactions of each ion with CaSR-mediated pathways. Strontium has a larger atomic radius than cal-

cium, which may result in a different activation profile of the CaSR. In addition, the possibility that cells respond to Sr²⁺ through mechanisms other than CaSR remains to be investigated. We recognize that to investigate the effect of Sr²⁺ independently of Ca²⁺ is challenging because

a)



b)

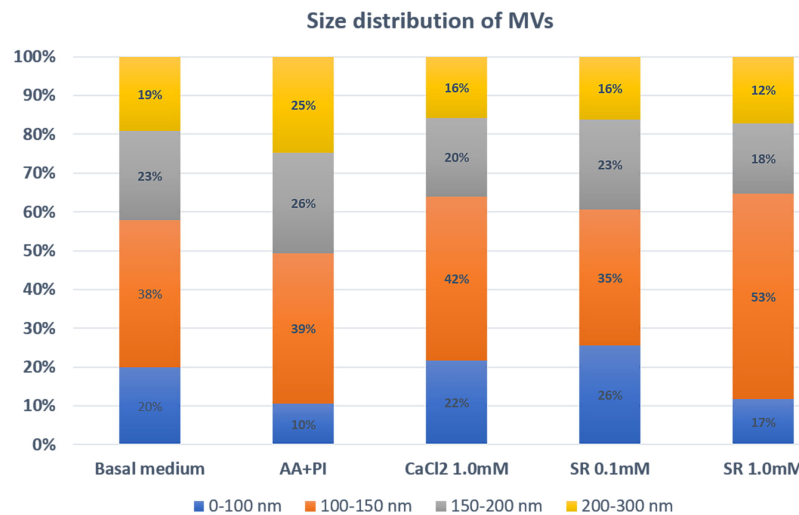


Fig. 4. Compared to osteogenic medium (AA+P_i) alone, Ca²⁺, as CaCl₂, or Sr²⁺, as SR, inhibits matrix vesicle (MV) secretion by 17IIA11 cells but sustains the average MV size (100–150 nm). (a) Based on NTA analysis, the total MVs released per cell were obtained. (b) Size distribution (%) analysis of MVs ranging from 0 to 300 nm. The number inside the bars represents the percentage of MVs associated with the size corresponding to the colors, as follows: 0–100 nm (blue), 100–150 nm (orange), 150–200 nm (grey), and 200–300 nm (yellow).

(1) cytosolic calcium levels are high, and (2) the culture medium also contains calcium. Consequently, the observed results may reflect a synergistic interaction between Sr²⁺ and Ca²⁺ rather than the effect of Sr²⁺ alone. Similar to this work, recent studies highlighted the dose-dependent activation of the Erk1/2 pathway by Sr²⁺ [45,113,114]. Further studies must be able to exploit aspects of this area to mitigate the effect of calcium, but also should be careful, since calcium is a secondary messenger involved in many cellular events. Additionally, the use of inhibitors for Erk (U0126) and CREB (KG-501) would greatly help to study the interplay of both pathways to the MV release and biomineralization process.

Furthermore, triggering the Erk1/2 and CREB pathways influences the expression levels of mRNAs encoding key osteogenic markers [51,115,116]. Thus, we investigated whether the activation of these pathways influences the expression of *Runx2*, *Sp7*, *collagen alpha 1*, and *TNAP*, as well as *Smpd3* and *PHOSPHO1* phosphatases (Supplementary Figs. 2,3). Quantitative PCR revealed that neither Ca²⁺ nor Sr²⁺ produced substantial time-dependent changes in the mRNA levels of osteogenesis-related genes.

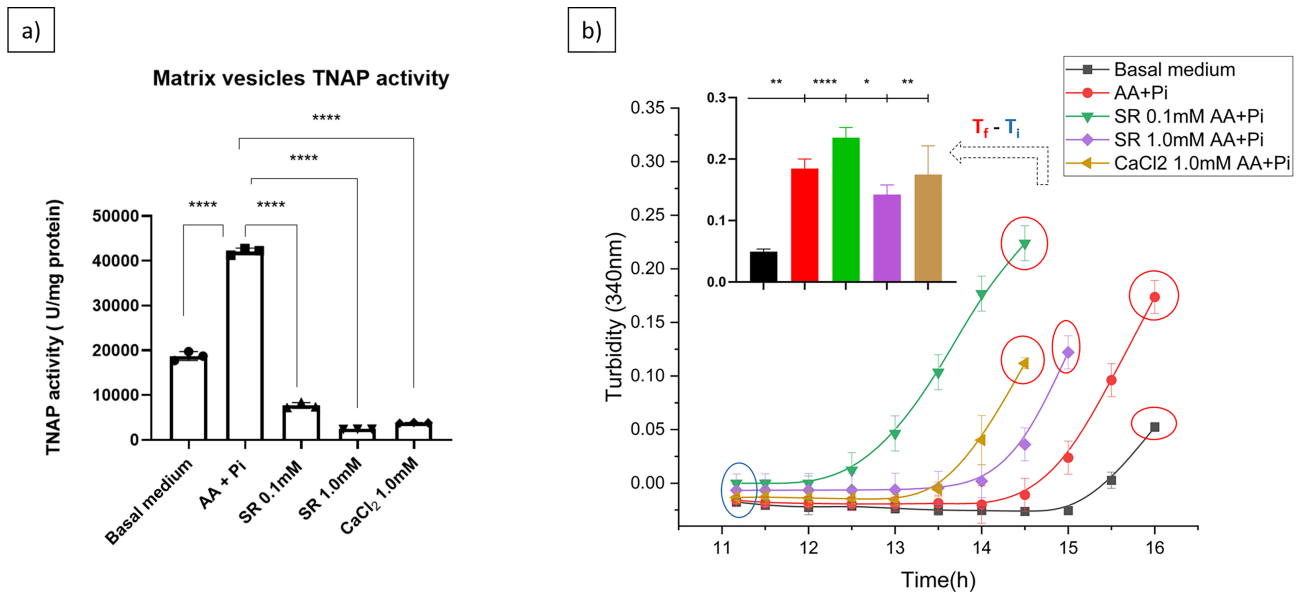


Fig. 5. Tissue non-specific alkaline phosphatase (TNAP) activity measured in MVs isolated from 17IIA11 cells increases in osteogenic medium (AA+Pi) compared to basal medium or Ca^{2+} , as CaCl_2 , or Sr^{2+} , as SR. (a) TNAP activity in MVs isolated from 17IIA1 cells was assessed as described previously [118]. Multiple statistical comparisons were performed by one-way ANOVA, p values **** $p < 0.0001$. (b) Changes in turbidimetry (340 nm) as a function of incubation time in synthetic cartilage lymph (SCL) were followed for 20 h (mineralization curve). Higher turbidity can be assigned to greater mineral deposition. The insert represents the statistical analysis for the final mineralization time (T_f) minus the initial time (T_i) as described here [28]. One-way ANOVA was used to determine the statistically significant differences in the reaction time for each group. p values * $p < 0.05$, ** $p < 0.005$, **** $p < 0.0001$.

3.3 Sr^{2+} Affects MV Release and MV-Supported Mineral Formation

Chaudhary *et al.* (2016) [78] described that mineralization-supporting ions, in particular P_i , are stimulators of MVs release from mineralization-competent cells. At the molecular level, P_i mediates MV release by activating the Erk1/2 signaling pathway, which is followed by actin fiber reorganization. Also, the MV protein composition changes in the presence of ions compared to MVs in the presence of classic osteogenic factors alone. Bechhoff *et al.* (2008) [117] reported how Sr^{2+} affects MVs. Specifically, these authors demonstrated that Sr^{2+} negatively affects mineral growth induced by MVs. Whereas earlier work stimulated isolated MVs with SR before functional analysis, our experimental design differed in that we initially exposed 17IIA11 cells to 1.0 mM Ca^{2+} or to 0.1- or 1.0-mM Sr^{2+} in osteogenic medium for 24 h, and subsequently quantified MV production and activity. First, we investigated how Ca^{2+} or Sr^{2+} in osteogenic medium affected MV size and concentration by quantitative NTA (Supplementary Fig. 4). Fig. 4a,b represent MV release per cell and size distribution.

We firstly observed that 17IIA11 cells naturally secrete MVs under standard culture conditions, and this secretion is further enhanced when the cells are placed in osteogenic medium (Fig. 4). Addition of 1.0 mM Ca^{2+} or 0.1 or 1.0 mM Sr^{2+} to osteogenic medium decreased MV release per cell (Fig. 4a) but did not change MV size (Fig. 4b)

compared to osteogenic medium alone. The MV diameters were mostly in the 100–150 nm range, followed by 150–200 nm, which is characteristic of MVs [1]. In osteogenic medium and 1.0 mM Ca^{2+} or Sr^{2+} , the percentage of MVs with diameters ranging from 100 to 150 nm increased (Fig. 4b).

The amount of MVs released by 17IIA11 cells is not directly correlated with the mineralization function—MV function is dictated by MV molecular composition. Thus, to assess the mineralization potential of MVs released from 17IIA11 cells under different conditions, we measured the activity of TNAP (Fig. 5a, Ref. [28,118]), a critical enzyme for biomineralization [119,120]. As anticipated, TNAP activity was elevated in osteogenic medium relative to standard culture conditions. However, when Ca^{2+} or Sr^{2+} was added—regardless of the concentration tested, TNAP activity was markedly reduced compared with cells maintained in standard growth medium (Fig. 5a). Despite the lower TNAP activity and reduced MV release, the addition of 0.1 mM Sr^{2+} to the osteogenic medium enhanced mineral precipitation (Fig. 5b) as evidenced by increased turbidity at 340 nm [28,79]. These findings indicate that increased MV abundance or TNAP activity does not necessarily correlate with greater mineralization capacity. In contrast, mineral propagation efficiency was lower in basal or osteogenic medium alone, even though both TNAP activity and MV release were higher under these conditions. Moreover, supplementation with 1.0 mM Ca^{2+} or Sr^{2+} in the osteogenic

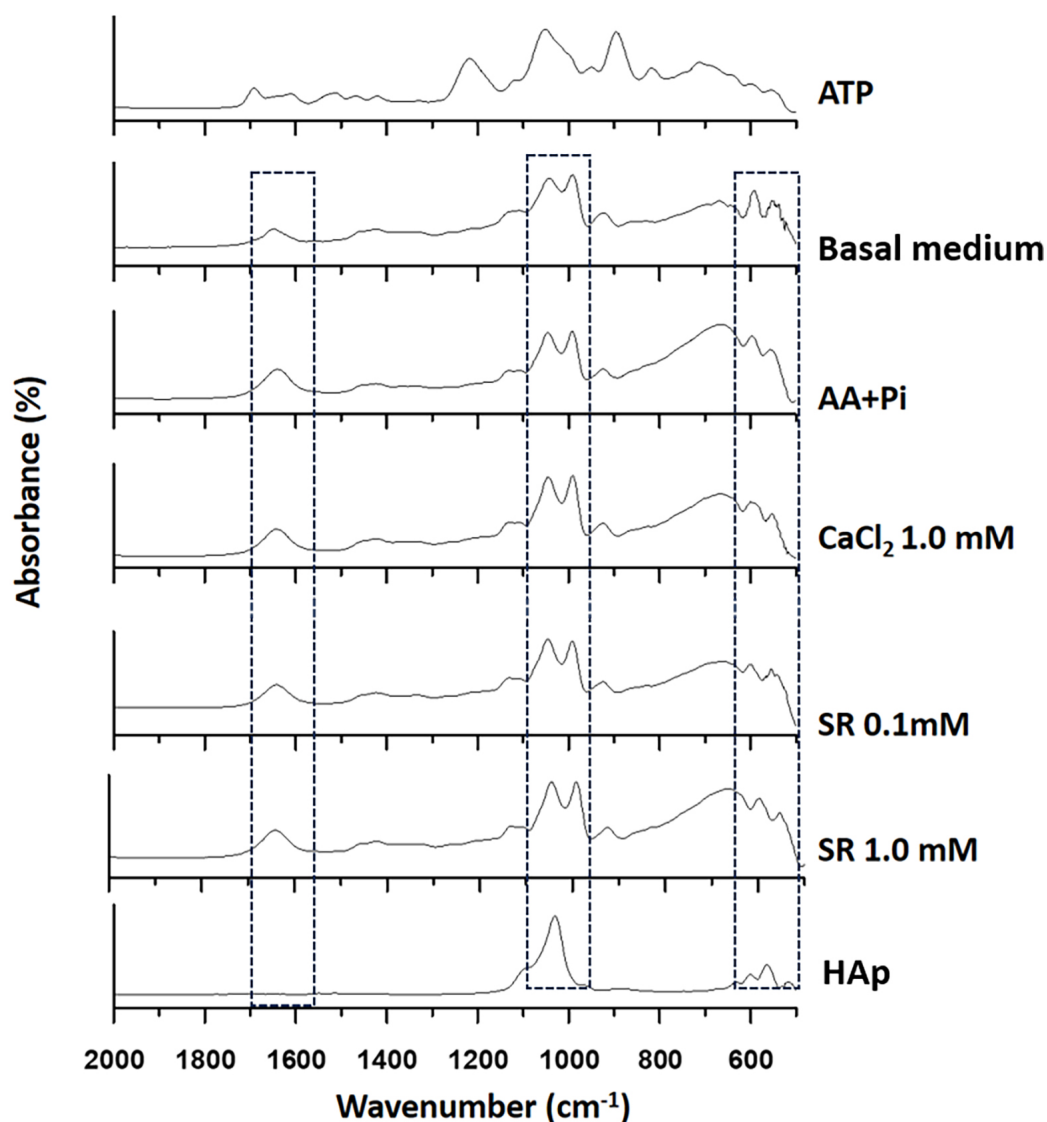


Fig. 6. Mineral composition assessed by ATR-FTIR spectra, which display the characteristic peaks of hydroxyapatite (HAp) ($\sim 1047 \text{ cm}^{-1}$). ATR-FTIR described the spectra for MVs extracted from basal medium; osteogenic medium (AA+Pi); 0.1 or 1.0 mM Ca^{2+} , as CaCl_2 ; or 0.1 or 1.0 mM Sr^{2+} , as SR, in osteogenic medium. For comparison, the ATR-FTIR spectra of HAp and ATP are presented. The dashed lines represent the peaks used to analyze the mineral phase. Data are reported as the mean of three independent ATR-FTIR spectra.

medium produced a more efficient mineralization response than basal medium or osteogenic medium alone (Fig. 5b).

ATR-FTIR spectroscopy was used to analyze the chemical composition of the minerals formed in the presence of MVs incubated in synthetic cartilage lymph (SCL) buffer containing ATP, a natural substrate for TNAP (Fig. 6).

The ATR-FTIR spectra showed that the minerals obtained after incubating MVs in SCL exhibited the characteristic vibrational peaks of HAp [121]. The intense peaks at 1040 and 940 cm^{-1} are related to asymmetric stretching of the PO_4^{3-} group and HPO_4^{2-} , a precursor of apatite. Comparison with the spectrum of ATP clearly shows that this substrate was completely consumed. Indeed, the spec-

trum of the resulting minerals did not display the typical peaks of ATP.

3.4 MVs Contain Proteins That Support Mineralization, and Their Morphology Changes Upon the Addition of Different Ions

Western blot helped to analyze the presence of lysosomal membrane glycoprotein (Lamp1), AnxV, and TNAP, which are proteins usually found in mineralization-competent MVs [78] (Fig. 7).

TNAP participates in P_i formation, and AnxV has been associated with Ca^{2+} transport from the extracellular environment to the MV lumen [15,122]. The role played by these proteins in biomineralization has also been stud-

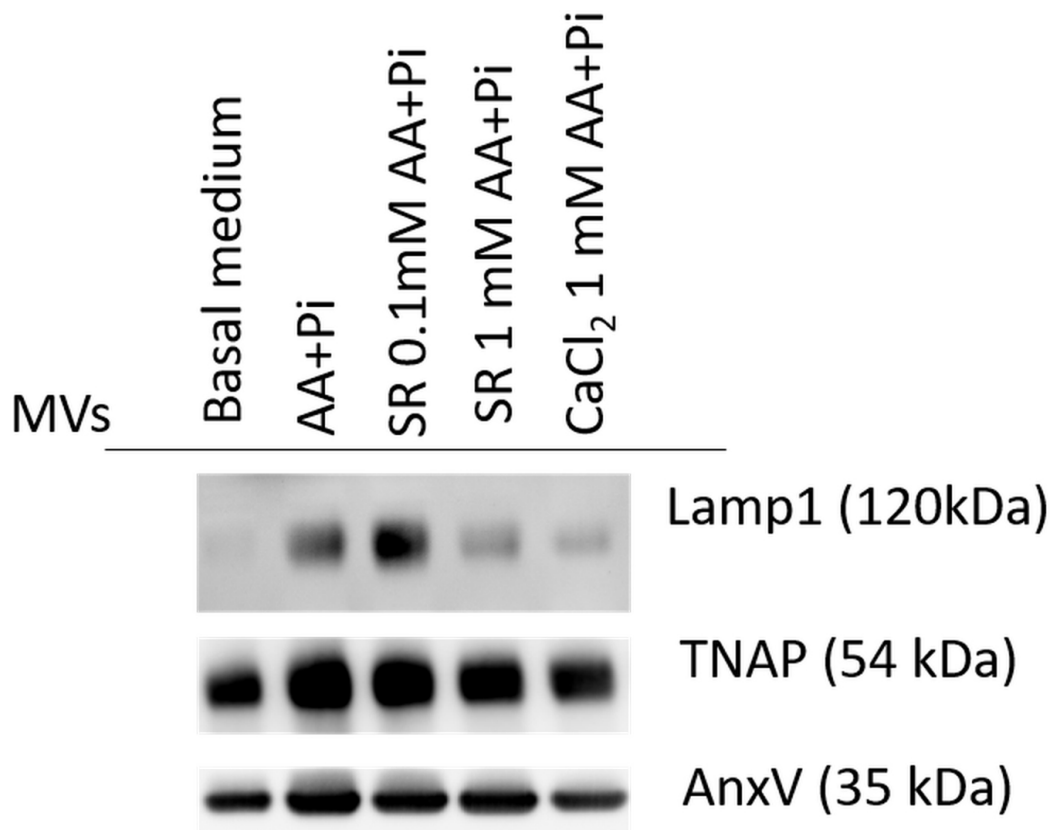


Fig. 7. Western blot analysis of mineralization-supporting proteins in MVs. MVs derived from 17IIA11 cells exposed to basal medium, osteogenic medium, Ca^{2+} , as CaCl_2 or Sr^{2+} , as SR, are enriched in proteins that support mineralization: TNAP and AnxV, and the cytosolic and cell organelle protein Lamp1. Lysosomal marker, Lamp1, is poorly expressed in 17IIA11 cells exposed to basal medium or Sr^{2+} , as SR, in osteogenic medium.

Table 1. Parameters derived from AFM revealed protrusions in the membrane of MVs derived from 17IIA11 cells stimulated with Ca^{2+} , as CaCl_2 , or Sr^{2+} , as SR, and zeta potential.

| Vesicles | Medium diameter AFM (nm) | Medium height AFM (nm) | Protrusion height (nm)* | Mean roughness | Zeta potential (mV) |
|------------------------|--------------------------|---------------------------|-------------------------|---------------------------|---------------------------|
| Basal medium | 101.1 ± 0.1 **** | 8.38 ± 0.03 ^{ns} | - | 0.84 ± 0.24 ^{ns} | -25.6 ± 3.0 ^{ns} |
| AA+Pi | 164.3 ± 0.1 | 8.62 ± 0.10 | - | 0.90 ± 0.23 | -22.2 ± 1.6 ^{ns} |
| SR 0.1 mM | 175.0 ± 0.1 **** | 22.71 ± 0.50 **** | 14.91 | 1.13 ± 0.27 ^{ns} | -23.5 ± 1.2 ^{ns} |
| SR 1.0 mM | 130.1 ± 0.1 **** | 3.55 ± 0.20 **** | 7.30 | 0.64 ± 0.35 ^{ns} | -21.9 ± 1.0 ^{ns} |
| CaCl_2 1.0 mM | 158.41 ± 0.1 **** | 6.50 ± 0.10 **** | 5.88 | 0.68 ± 0.30 ^{ns} | -20.4 ± 0.5 ^{ns} |

AFM helped to study the MV medium diameter (nm), medium height, presence or absence of protrusion, and ratio roughness. Zeta potential analysis (mV) was used to measure the overall MV surface charge. The presence of protrusion suggests a change in the MV membrane viscoelastic properties, which is often associated with nucleation. The ratio roughness regards the MV membrane fluidity. One-way ANOVA was used to determine the statistically significant differences for each group (**** $p < 0.0001$). Superscript represents the statistical analysis for each sample compared to the osteogenic medium. *Protrusion size corresponds to the maximum peak reached by the protuberance. ^{ns}, not significant.

ied [123,124]. In this study, we detected these proteins in 17IIA11 cells maintained in basal medium and identified only a single TNAP isoform. This contrasts with previous findings showing that MVs isolated from 17IIA11 cells cultured in osteogenic medium contain at least three distinct TNAP isoforms [78]. Regarding Lamp1, a protein typically detected in MVs derived from 17IIA11 cells, its expression was low in cells cultured either in basal medium or in os-

teogenic medium supplemented with Sr^{2+} (0.1 or 1.0 mM). The role played by Lamp1 in biomineralization must be further investigated, but it has been described to participate in pH regulation in lysosomes [125]. Given that pH affects HAp synthesis and deposition [126], Lamp1 may indirectly affect biomineralization.

Afterward, we evaluated MVs' morphology by AFM and TEM (Fig. 8) and analyzed their surface charge by zeta

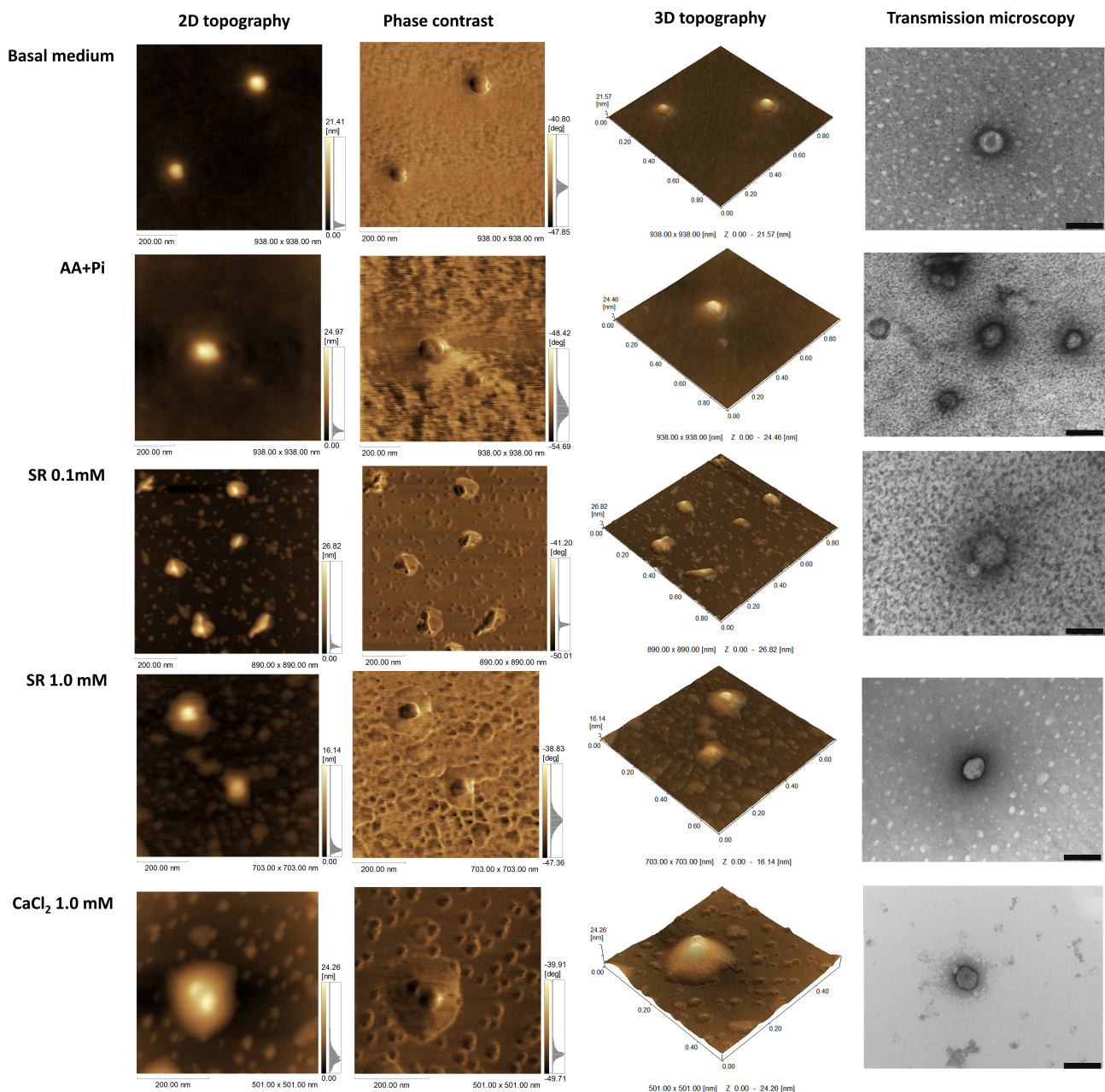


Fig. 8. Atomic force microscopy (AFM) and transmission electron microscopy (TEM) reveal a change in the membrane fluidity of MVs. From left to right: 2D topography, phase contrast, 3D topography, and TEM images. For each sample, 100 MVs were analyzed. TEM scale bar (black) corresponds to 200 nm.

potential (Table 1). AFM is a powerful technique to investigate particle structure at the nanometric scale based on high-resolution images [127]. AFM-based techniques also enable qualitative assessment of differences in sample viscoelasticity through the interaction between the probe tip and the sample surface. In addition, AFM imaging provides quantitative parameters such as surface roughness, mean diameter, and mean height. This approach has previously been used to characterize MVs [128–130].

MVs derived from 17HIA11 cells exposed to Sr^{2+} (0.1 or 1.0 mM) or Ca^{2+} (1.0 mM) in osteogenic medium dis-

played structural alterations in their outer membrane. These were evidenced by the presence of protrusions (darker regions) with distinct viscoelastic properties, as revealed by variations in the phase-contrast imaging (Fig. 8). Such protrusions could barely be identified in the MVs exposed to basal medium or osteogenic medium alone. In addition, we calculated a series of parameters from AFM data as described in Table 1.

The MVs exhibited an overall diameter of approximately 100–200 nm, consistent with the NTA measurements (Fig. 4b). The average height of the surface protru-

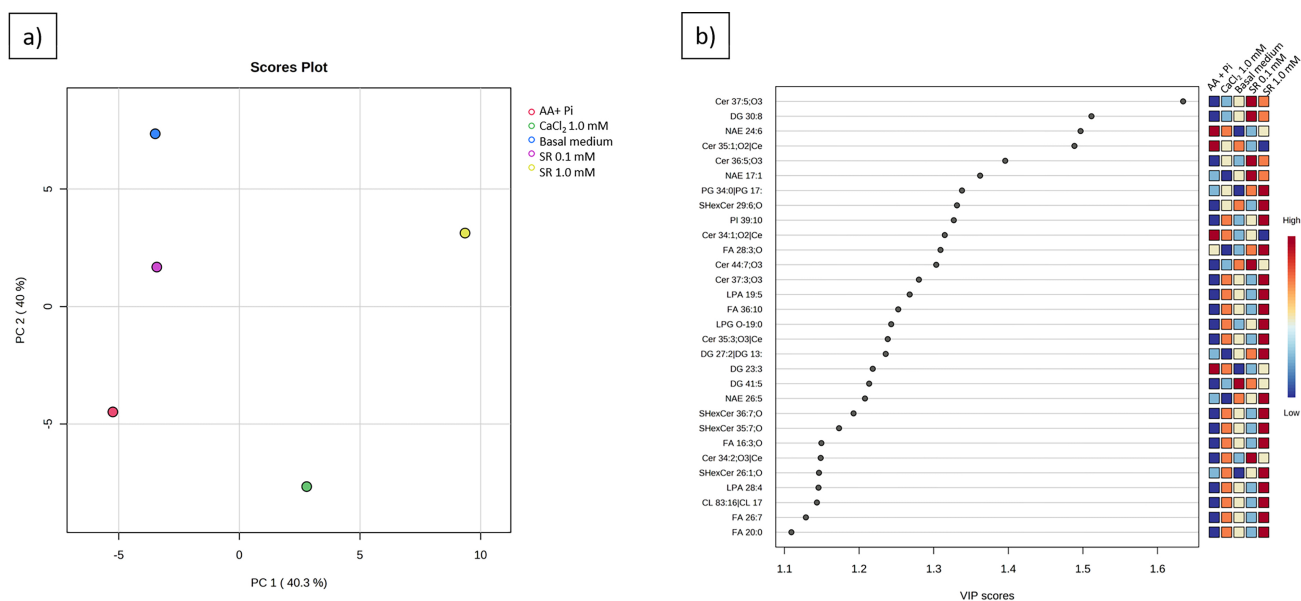


Fig. 9. MVs derived from 17IIA11 cells stimulated with basal medium, osteogenic medium (AA+Pi); Ca²⁺, as CaCl₂, in osteogenic medium, or Sr²⁺, as SR were subjected to lipidomic analysis. (a) The lipidomic principal component analysis score plot (PCA) reveals heterogeneity between the stimulations, which indicates diversity in the lipid profile of each group. (b) Variable importance in projection (VIP) plot analysis of 30 lipids demonstrates that MVs derived from 17IIA11 cells stimulated with Sr²⁺, as SR, in osteogenic medium are highly enriched in Cer. The 30 most differently regulated lipids vary among the groups, and their expression is indicated in the color panel. Highly expressed (dark red) and mildly expressed (dark blue) lipids.

sions varied depending on the stimulus. Notably, MVs isolated from 17IIA11 cells stimulated with 0.1 mM Sr²⁺ in osteogenic medium displayed a greater average height and more prominent protrusions (14.91 nm). Such elevated protrusions correspond to a wider range of phase shifts in MV topology, indicating increased protein and lipid complexity, as previously reported [130].

3.5 Lipidomic Analysis Reveals a Change in the MV Lipid Profile

The lipid composition modulates the catalytic activity of enzymes incorporated at the MV bilayer, directly affecting the MV biomineralization ability [79]. Our AFM data pointed to altered viscoelastic properties of the MV membrane, and a change in the MV mineralization profile (Fig. 5b). Therefore, we evaluated the overall lipid content in the MVs by lipidomic analysis. We started by analyzing the principal component analysis (PCA) (Fig. 9a), which demonstrated heterogeneity among the MV groups. The analysis described 51% of the total variance, which included 42.8% of principal component 1 and 8.2% of principal component 2, whereby component 1 was the major component of discrimination.

We then selected the 30 most differentially regulated lipids among the MVs, as shown in the variable importance in projection (VIP) plot (Fig. 9b). Several lipid species, including N-acyl ethanolamines (NAE), phosphatidylinositols (PI), FA, ceramides (Cer), lysophosphatidic acids (LPA), sulfatide hexosylceramides (SHexCer), diacylglyc-

erols (DGs), and lysophosphatidylglycerols (LPG), were modulated. The heat map in Fig. 10 illustrates the global lipid profile extracted from each MV sample.

The MVs contained 81 identifiable lipid species (Fig. 10), and their lipid class distribution varied depending on the ionic stimulus. MVs derived from 17IIA11 cells exposed to 0.1 mM Sr²⁺ in osteogenic medium were enriched in Cer, DG, SM, and a wide variety of FA. Similarly, MVs obtained from cells stimulated with 1.0 mM Sr²⁺ showed a lipid profile comparable to that of the 0.1 mM Sr²⁺ group, but with higher levels of LPG, PI, phosphatidylethanolamine (PE), and LPA. MVs released under basal medium conditions displayed a lipid composition similar to the Sr²⁺-stimulated groups. In contrast, MVs isolated from cells cultured in osteogenic medium alone exhibited elevated Cer and SM content. Finally, MVs from cells treated with 1.0 mM Ca²⁺ in osteogenic medium were NAE along with other lipid species.

Additionally, we generated pie charts to visualize how lipid class proportions shifted in response to each treatment (Fig. 11). The MV membrane is enriched in phospholipids, SM, and cholesterol [12]. Here, various lipids were present in the MV membranes, including lysophosphatidylcholine (LPC), PE, phosphocholine (PA), PI, PS, sphingomyelin (SM), Cer, hexosylceramide (HexCer), and free cholesterol (FC; sterol). Cardiolipin (CL), a lipid predominantly located in inner mitochondrial membranes, was also present. The MV membranes also contained storage lipids, including sterol (ST), DG, and triacylglycerol (TG).

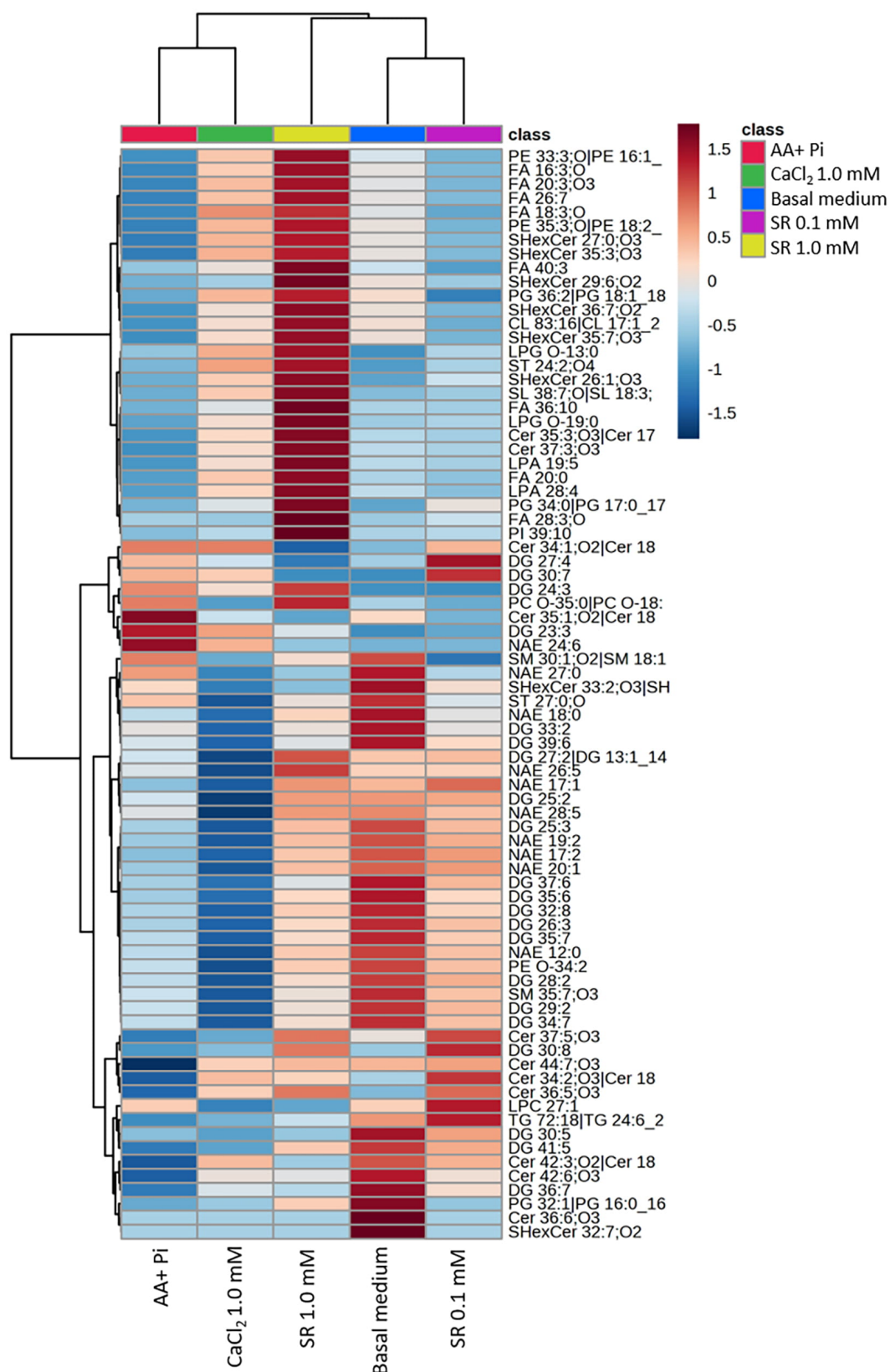


Fig. 10. A heat map of 81 lipids shows that the lipid composition of MVs varies depending on the stimulus applied to 17HIA11 cells. All 81 lipids are associated with the MV membrane. The color scale ranges from high (dark red) to low (dark blue) abundance, indicating the relative expression level of each lipid across the experimental groups.

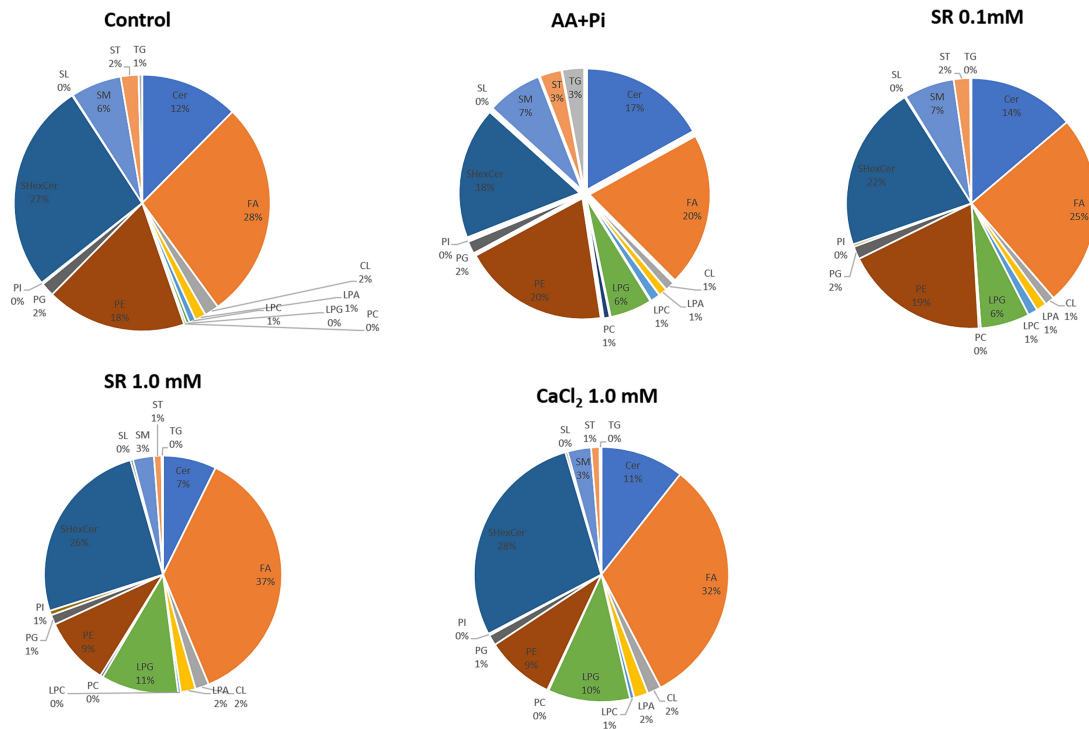


Fig. 11. The pie charts illustrate the impact of various treatments on overall lipid expression. TG, triacylglycerol; DG, diacylglycerol; FA, fatty acid; ST, sterol lipids; PC, phosphatidylcholine; PE, phosphatidylethanolamine; CL, cardiolipin; PI, phosphatidylinositol; SL, saccharolipid; PG, phosphatidylglycerol; LPC, lysophosphatidylcholine; LPA, lysophosphatidic acid; LPG, lysophosphatidylglycerol; SM, sphingomyelin; Cer, ceramide.

Apart from structural and storage roles, sphingolipids serve as bioactive signaling molecules and are involved in many biological regulations, like inflammation, cell death, and proliferation [131]. In the context of MVs and bone physiology, this class of lipids, together with cholesterol and PS, is extremely important because they are involved with anchoring and regulating key proteins, e.g., TNAP; organizing the lipid bilayer; and creating lipid microdomains (lipid rafts). A better understanding of how sphingolipids and cholesterol regulate MV proteins and help to coordinate lipids throughout the MV membrane can be reviewed elsewhere [132–138].

In this context, SM and Cer occur in healthy bone tissue and are required for normal mineralization to take place, so their presence in the lipidome of mineral-competent MVs is not surprising [139]. Osteoporotic mice present lower SM and Cer levels in the femur [140], which attests to the role of these lipids in healthy bone homeostasis. Cer, a potent signaling molecule, is pro-apoptotic [141]. Cer hydrolysis to sphingosine mediated by Sphingomyelin Phosphodiesterase 3 (Smpd3) is accompanied by phosphorylation to ceramide-1-phosphate and sphingosine-1-phosphate, which are important bioactive molecules modulating biological processes, such as cell proliferation, apoptosis, migration, and adhesion [131]. Moreover, *in situ* SM catabolism is needed for mineralizing bone and dentin; hence, *in vitro* MV-mediated mineralization is associated

with SM being rapidly degraded [14]. Additionally, mature osteoblasts have higher expression of Smpd3, a key enzyme in SM hydrolysis to PC and Cer [142,143]. A similar effect has been observed in odontoblasts [144]. Even though SM and Cer are relevant for bone physiology, their roles in MVs are not fully understood. SM hydrolysis to PA and Cer has been hypothesized to increase free PO_4^{3-} concentration in the MV vicinity, thereby favoring the onset of mineralization [139].

Importantly, these compositional shifts in lipid profile correlate with the structural alterations observed by phase-contrast imaging as described in the AFM and TEM panel (Fig. 8). We demonstrated that MVs derived from 17IIA11 cells exposed to Sr^{2+} (0.1 or 1.0 mM) or Ca^{2+} (1.0 mM) in osteogenic medium exhibited distinct outer-membrane protrusions—visible as darker regions with differing viscoelastic properties. These protrusions were minimal or absent in MVs from cells maintained in basal or osteogenic medium alone. Collectively, the data suggest that ion-dependent remodeling of MV lipid composition—particularly changes in Cer, SM, PE/PI/LPA species, and NAE—is associated with alterations in MV membrane architecture. The presence of specific lipid enrichments under Sr^{2+} and Ca^{2+} stimulation likely contributes to the formation of the protrusions observed, reflecting changes in membrane rigidity, curvature, and organization.

Finally, MVs isolated from 17IIA11 cells exposed to 1.0 mM Ca^{2+} or to 0.1- or 1.0-mM Sr^{2+} showed greater mineralizing capacity (Fig. 5b) and were characterized by elevated levels of SM and Cer (Fig. 11). **Supplementary Table 1** provides a summary of the key findings shown here.

4. Conclusions

SR has been used as a potential drug aimed at bone fractures since 1870, but its prescription for osteoporotic patients was only made possible years later (1960). Since then, the Sr^{2+} biochemical mechanism has been widely investigated. Its anabolic effect in promoting bone turnover and its inhibitory effect on osteoclast activity make SR a strong candidate for treating osteoporosis and other bone-related diseases. However, the intrinsic mechanisms involved in these processes are not fully understood. Mineral deposition in the ECM mediated by MVs is also poorly understood. Here, we have investigated how Sr^{2+} affects MV release and function. Additionally, for the first time, we have studied the MV lipid profile by lipidomic analysis and evaluated how it is affected by Sr^{2+} . For comparison purposes, we have also evaluated Ca^{2+} , whose function in mineralization is well established. In contrast with other works, here we stimulated the cells with different SR or CaCl_2 concentrations and isolated the MVs. The effect of SR and CaCl_2 on osteocompetent cells (more so in osteoblasts) is well described, but no one has ever paid attention to or fully characterized the MVs released by preodontoblast cells. Given that MVs are nanoreactors that can bind to collagen and deposit HAp, characterizing them in the presence of different stimuli (e.g., osteoinductors-hormones, BMP, biomaterials, ions, etc.) is pivotal.

The multifaceted influence of Sr^{2+} on mineralization became evident in our study. At the molecular level, we found that extracellular mineral deposition is highly dependent on Sr^{2+} concentration, with lower concentrations enhancing mineral formation and higher concentrations suppressing it. Among the pathways examined, Erk1/2 and CREB signaling were sensitive to changes in Sr^{2+} levels, whereas the expression of osteogenic genes in 17IIA11 cells remained largely unaffected. Whether Sr^{2+} activates CaSR or other ion-sensing receptors remains elusive. Additionally, Sr^{2+} reduces MV release and TNAP activity, while maintaining highly efficient mineral deposition, as indicated by turbidimetry analysis. The lipid composition of MVs varied according to both the type and concentration of the stimulating ion, supporting the notion that the parental cells sense these ionic cues and adjust MV lipid profiles accordingly. Indeed, the heat map indicates that Ca^{2+} and Sr^{2+} differentially alter MV lipid composition, which in turn is reflected in changes to MV release and mineralization efficiency. In this sense, SR acts as an anabolic drug that can activate many osteogenic pathways and interfere with MV release and efficiency by modulating the lipid content of MV.

Availability of Data and Materials

The datasets used and analyzed during the current study are available from the corresponding author on reasonable request.

Author Contributions

LH, APR, and DN conceived the study; APR and DN supervised the study; LH, MS, JGC and SM designed experiments; LH, MS, LHSA, and JGC performed experiments; AFLV and SM helped with the lipidomic experiment and analysis; LH, PC, APR, SM and DN analyzed data; PC, APR, SM, and DN made manuscript revisions. All authors contributed to editorial changes in the manuscript. All authors read and approved the final manuscript. All authors have participated sufficiently in the work and agreed to be accountable for all aspects of the work.

Ethics Approval and Consent to Participate

The 17IIA11 cell line used in this study was obtained from Prof. Dr. Odile Kellermann and Prof. Dr. Anne Poliard, Laboratoire de Différenciation Cellulaire et Prions-UPR, France. As this study involved only in vitro experiments using an established cell line and did not include the collection of new human or animal samples, ethical approval was not required according to the regulations of the Institutional Animal Care and Use Committee of the University of Pittsburgh.

Acknowledgment

We want to express our sincere gratitude to Professor Carlos Sorgi of the Department of Chemistry, Faculty of Philosophy, Sciences, and Letters at Ribeirão Preto, University of São Paulo, for his invaluable assistance and expertise in lipidomic analysis. His technical guidance, attention to detail, and insightful feedback greatly enhanced the quality and depth of this work. We are deeply appreciative of the time and effort he dedicated to ensuring the success of this project.

Funding

This work was supported by the Fundação de Amparo à Pesquisa do Estado de São Paulo (grant number 2019/25054-2, 22/04885-6, 2019/25054-2, LH, JGC, LHSA, PC, and APR, respectively); the National Institute of Dental and Craniofacial Research (grant number DE023083, F32DE029096, DN and MS, respectively).

Conflict of Interest

The authors declare no conflict of interest.

Supplementary Material

Supplementary material associated with this article can be found, in the online version, at <https://doi.org/10.31083/FBL47664>.

References

- [1] Bottini M, Mebarek S, Anderson KL, Strzelecka-Kiliszek A, Bozycski L, Simão AMS, *et al.* Matrix vesicles from chondrocytes and osteoblasts: Their biogenesis, properties, functions and biomimetic models. *Biochimica et Biophysica Acta. General Subjects*. 2018; 1862: 532–546. <https://doi.org/10.1016/j.bbagen.2017.11.005>.
- [2] Hale JE, Wuthier RE. The mechanism of matrix vesicle formation. Studies on the composition of chondrocyte microvilli and on the effects of microfilament-perturbing agents on cellular vesiculation. *The Journal of Biological Chemistry*. 1987; 262: 1916–1925.
- [3] Rabinovitch AL, Anderson HC. Biogenesis of matrix vesicles in cartilage growth plates. *Federation Proceedings*. 1976; 35: 112–116.
- [4] Borg TK, Runyan R, Wuthier RE. A freeze-fracture study of avian epiphyseal cartilage differentiation. *The Anatomical Record*. 1981; 199: 449–457. <https://doi.org/10.1002/ar.1091990402>.
- [5] Akisaka T, Shigenaga Y. Ultrastructure of growing epiphyseal cartilage processed by rapid freezing and freeze-substitution. *Journal of Electron Microscopy*. 1983; 32: 305–320.
- [6] Anderson HC, Garimella R, Tague SE. The role of matrix vesicles in growth plate development and biomineralization. *Frontiers in Bioscience*. 2005; 10: 822–837. <https://doi.org/10.2741/1576>.
- [7] Magne D, Bluteau G, Fauchoux C, Palmer G, Vignes-Colombeix C, Pilet P, *et al.* Phosphate is a specific signal for ATDC5 chondrocyte maturation and apoptosis-associated mineralization: possible implication of apoptosis in the regulation of endochondral ossification. *Journal of Bone and Mineral Research*. 2003; 18: 1430–1442. <https://doi.org/10.1359/jbmr.2003.18.8.1430>.
- [8] Rilla K, Pasonen-Seppänen S, Deen AJ, Koistinen VVT, Wojciechowski S, Oikari S, *et al.* Hyaluronan production enhances shedding of plasma membrane-derived microvesicles. *Experimental Cell Research*. 2013; 319: 2006–2018. <https://doi.org/10.1016/j.yexcr.2013.05.021>.
- [9] Garcés-Ortiz M, Ledesma-Montes C, Reyes-Gasga J. Presence of matrix vesicles in the body of odontoblasts and in the inner third of dentinal tissue: a scanning electron microscopic study. *Medicina Oral, Patología Oral Y Cirugía Bucal*. 2013; 18: e537–e541. <https://doi.org/10.4317/medoral.18650>.
- [10] Abdallah D, Hamade E, Merhi RA, Bassam B, Buchet R, Mebarek S. Fatty acid composition in matrix vesicles and in microvilli from femurs of chicken embryos revealed selective recruitment of fatty acids. *Biochemical and Biophysical Research Communications*. 2014; 446: 1161–1164. <https://doi.org/10.1016/j.bbrc.2014.03.069>.
- [11] Balcerzak M, Malinowska A, Thouverey C, Sekrecka A, Dadlez M, Buchet R, *et al.* Proteome analysis of matrix vesicles isolated from femurs of chicken embryo. *Proteomics*. 2008; 8: 192–205. <https://doi.org/10.1002/pmic.200700612>.
- [12] Lingwood D, Simons K. Lipid rafts as a membrane-organizing principle. *Science*. 2010; 327: 46–50. <https://doi.org/10.1126/science.1174621>.
- [13] Simão AMS, Bolean M, Favarin BZ, Veschi EA, Tovani CB, Ramos AP, *et al.* Lipid microenvironment affects the ability of proteoliposomes harboring TNAP to induce mineralization without nucleators. *Journal of Bone and Mineral Metabolism*. 2019; 37: 607–613. <https://doi.org/10.1007/s00774-018-0962-8>.
- [14] Wu LNY, Genge BR, Kang MW, Arsenault AL, Wuthier RE. Changes in phospholipid extractability and composition accompany mineralization of chicken growth plate cartilage matrix vesicles. *The Journal of Biological Chemistry*. 2002; 277: 5126–5133. <https://doi.org/10.1074/jbc.M107899200>.
- [15] Bolean M, Simão AMS, Barioni MB, Favarin BZ, Sebinelli HG, Veschi EA, *et al.* Biophysical aspects of biomineralization. *Biophysical Reviews*. 2017; 9: 747–760. <https://doi.org/10.1007/s12551-017-0315-1>.
- [16] Balcerzak M, Radisson J, Azzar G, Farlay D, Boivin G, Pikula S, *et al.* A comparative analysis of strategies for isolation of matrix vesicles. *Analytical Biochemistry*. 2007; 361: 176–182. <https://doi.org/10.1016/j.ab.2006.10.001>.
- [17] Sidorov AV. Mollusk *Lymnaea stagnalis* locomotor activity during feeding, the role of pH of hemolymph. *Zhurnal Evolutsionnoi Biokhimii i Fiziologii*. 2006; 42: 36–40. (In Russian)
- [18] Hayann L, Melo MT, Bahia Nogueira LF, Ciancaglini P, Bottini M, Ramos AP. Working with mineralizing extracellular vesicles. Part V: Use of Mineralizing extracellular vesicles in bone regeneration. In Bottini M, Ramos AP (eds.) *Mineralizing Vesicles* (pp. 385–405). Elsevier: Amsterdam. 2024. <https://doi.org/10.1016/B978-0-323-99158-2.00013-9>.
- [19] Hayann L, Ciancaglini P, Ramos AP, Napierala D. Calcium and phosphate and their role in matrix vesicles: A biological view. In Bottini M, Ramos AP (eds.) *Mineralizing Vesicles* (pp. 151–173). Elsevier: Amsterdam. 2024. <https://doi.org/10.1016/B978-0-323-99158-2.00010-3>.
- [20] Chaudhary SC, Khalid S, Smethurst V, Monier D, Mobley J, Huet A, *et al.* Proteomic profiling of extracellular vesicles released from vascular smooth muscle cells during initiation of phosphate-induced mineralization. *Connective Tissue Research*. 2018; 59: 55–61. <https://doi.org/10.1080/03008207.2018.1444759>.
- [21] Orimo H. The mechanism of mineralization and the role of alkaline phosphatase in health and disease. *Journal of Nippon Medical School*. 2010; 77: 4–12. <https://doi.org/10.1272/jnms.77.4>.
- [22] Bielez B, Klaushofer K, Oberbauer R. Renal phosphate loss in hereditary and acquired disorders of bone mineralization. *Bone*. 2004; 35: 1229–1239. <https://doi.org/10.1016/j.bone.2004.08.009>.
- [23] Marini F, Giusti F, Iantomasi T, Brandi ML. Congenital Metabolic Bone Disorders as a Cause of Bone Fragility. *International Journal of Molecular Sciences*. 2021; 22: 10281. <https://doi.org/10.3390/ijms221910281>.
- [24] Reznikov N, Hoac B, Buss DJ, Addison WN, Barros NMT, McKee MD. Biological stenciling of mineralization in the skeleton: Local enzymatic removal of inhibitors in the extracellular matrix. *Bone*. 2020; 138: 115447. <https://doi.org/10.1016/j.bone.2020.115447>.
- [25] Thouverey C, Malinowska A, Balcerzak M, Strzelecka-Kiliszek A, Buchet R, Dadlez M, *et al.* Proteomic characterization of biogenesis and functions of matrix vesicles released from mineralizing human osteoblast-like cells. *Journal of Proteomics*. 2011; 74: 1123–1134. <https://doi.org/10.1016/j.jprot.2011.04.005>.
- [26] Cornely R, Rentero C, Enrich C, Grewal T, Gaus K. Annexin A6 is an organizer of membrane microdomains to regulate receptor localization and signalling. *IUBMB Life*. 2011; 63: 1009–1017. <https://doi.org/10.1002/iub.540>.
- [27] Yadav MC, Bottini M, Cory E, Bhattacharya K, Kuss P, Narisawa S, *et al.* Skeletal Mineralization Deficits and Impaired Biogenesis and Function of Chondrocyte-Derived Matrix Vesicles in Phospho1(-/-) and Phospho1/Pi t1 Double-Knockout Mice. *Journal of Bone and Mineral Research*. 2016; 31: 1275–1286. <https://doi.org/10.1002/jbmr.2790>.
- [28] Andrioli LHS, Sebinelli HG, Favarin BZ, Cruz MAE, Ramos AP, Bolean M, *et al.* NPP1 and TNAP hydrolyze ATP synergistically during biomineralization. *Purinergic Signalling*. 2023; 19: 353–366. <https://doi.org/10.1007/s11302-022-09882-2>.
- [29] Kirsch T, Nah HD, Demuth DR, Harrison G, Golub EE, Adams SL, *et al.* Annexin V-mediated calcium flux across membranes

is dependent on the lipid composition: implications for cartilage mineralization. *Biochemistry*. 1997; 36: 3359–3367. <https://doi.org/10.1021/bi9626867>.

- [30] Chavkin NW, Chia JJ, Crouthamel MH, Giachelli CM. Phosphate uptake-independent signaling functions of the type III sodium-dependent phosphate transporter, PiT-1, in vascular smooth muscle cells. *Experimental Cell Research*. 2015; 333: 39–48. <https://doi.org/10.1016/j.yexcr.2015.02.002>.
- [31] Ansari S, de Wildt BWM, Vis MAM, de Korte CE, Ito K, Hofmann S, *et al.* Matrix Vesicles: Role in Bone Mineralization and Potential Use as Therapeutics. *Pharmaceuticals*. 2021; 14: 289. <https://doi.org/10.3390/ph14040289>.
- [32] Azoidis I, Cox SC, Davies OG. The role of extracellular vesicles in biomineralisation: current perspective and application in regenerative medicine. *Journal of Tissue Engineering*. 2018; 9: 2041731418810130. <https://doi.org/10.1177/2041731418810130>.
- [33] Millán JL. The role of phosphatases in the initiation of skeletal mineralization. *Calcified Tissue International*. 2013; 93: 299–306. <https://doi.org/10.1007/s00223-012-9672-8>.
- [34] Lee K, Kim H, Jeong D. Microtubule stabilization attenuates vascular calcification through the inhibition of osteogenic signaling and matrix vesicle release. *Biochemical and Biophysical Research Communications*. 2014; 451: 436–441. <https://doi.org/10.1016/j.bbrc.2014.08.007>.
- [35] Yuan C, Ni L, Zhang C, Hu X, Wu X. Vascular calcification: New insights into endothelial cells. *Microvascular Research*. 2021; 134: 104105. <https://doi.org/10.1016/j.mvr.2020.104105>.
- [36] Kunitomi Y, Hara ES, Okada M, Nagaoka N, Kuboki T, Nakano T, *et al.* Biomimetic mineralization using matrix vesicle nanofragments. *Journal of Biomedical Materials Research. Part A*. 2019; 107: 1021–1030. <https://doi.org/10.1002/jbm.a.36618>.
- [37] Cappariello A, Loftus A, Muraca M, Maurizi A, Rucci N, Teti A. Osteoblast-Derived Extracellular Vesicles Are Biological Tools for the Delivery of Active Molecules to Bone. *Journal of Bone and Mineral Research*. 2018; 33: 517–533. <https://doi.org/10.1002/jbmr.3332>.
- [38] Wei Y, Tang C, Zhang J, Li Z, Zhang X, Miron RJ, *et al.* Extracellular vesicles derived from the mid-to-late stage of osteoblast differentiation markedly enhance osteogenesis in vitro and in vivo. *Biochemical and Biophysical Research Communications*. 2019; 514: 252–258. <https://doi.org/10.1016/j.bbrc.2019.04.029>.
- [39] Wei Y, Shi M, Zhang J, Zhang X, Shen K, Wang R, *et al.* Autologous Versatile Vesicles-Incorporated Biomimetic Extracellular Matrix Induces Biomineralization. *Advanced Functional Materials*. 2020; 30: 2000015. <https://doi.org/10.1002/adfm.202000015>.
- [40] Weng Z, Zhang B, Wu C, Yu F, Han B, Li B, *et al.* Therapeutic roles of mesenchymal stem cell-derived extracellular vesicles in cancer. *Journal of Hematology & Oncology*. 2021; 14: 136. <https://doi.org/10.1186/s13045-021-01141-y>.
- [41] Qiao Z, Greven J, Horst K, Pfeifer R, Kobbe P, Pape HC, *et al.* Fracture Healing and the Underexposed Role of Extracellular Vesicle-Based Cross Talk. *Shock*. 2018; 49: 486–496. <https://doi.org/10.1097/SHK.0000000000001002>.
- [42] Martins M, Ribeiro D, Martins A, Reis RL, Neves NM. Extracellular Vesicles Derived from Osteogenically Induced Human Bone Marrow Mesenchymal Stem Cells Can Modulate Lineage Commitment. *Stem Cell Reports*. 2016; 6: 284–291. <https://doi.org/10.1016/j.stemcr.2016.01.001>.
- [43] Palamà MEF, Shaw GM, Carluccio S, Reverberi D, Sercia L, Persano L, *et al.* The Secretome Derived From Mesenchymal Stromal Cells Cultured in a Xeno-Free Medium Promotes Human Cartilage Recovery *in vitro*. *Frontiers in Bioengineering and Biotechnology*. 2020; 8: 90. <https://doi.org/10.3389/fbioe.2020.00090>.
- [44] Bonnelye E, Chabadel A, Saltel F, Jurdic P. Dual effect of strontium ranelate: stimulation of osteoblast differentiation and inhibition of osteoclast formation and resorption in vitro. *Bone*. 2008; 42: 129–138. <https://doi.org/10.1016/j.bone.2007.08.043>.
- [45] Fromig   O, Ha   E, Barbara A, Petrel C, Traiffort E, Ruat M, *et al.* Calcium sensing receptor-dependent and receptor-independent activation of osteoblast replication and survival by strontium ranelate. *Journal of Cellular and Molecular Medicine*. 2009; 13: 2189–2199. <https://doi.org/10.1111/j.1582-4934.2009.00673.x>.
- [46] Riggs BL, Parfitt AM. Drugs used to treat osteoporosis: the critical need for a uniform nomenclature based on their action on bone remodeling. *Journal of Bone and Mineral Research*. 2005; 20: 177–184. <https://doi.org/10.1359/JBMR.041114>.
- [47] Ducy P, Zhang R, Geoffroy V, Ridall AL, Karsenty G. *Osf2/Cbfa1*: a transcriptional activator of osteoblast differentiation. *Cell*. 1997; 89: 747–754. [https://doi.org/10.1016/S0092-8674\(00\)80257-3](https://doi.org/10.1016/S0092-8674(00)80257-3).
- [48] Meunier PJ, Roux C, Seeman E, Ortolani S, Badurski JE, Spector TD, *et al.* The effects of strontium ranelate on the risk of vertebral fracture in women with postmenopausal osteoporosis. *The New England Journal of Medicine*. 2004; 350: 459–468. <https://doi.org/10.1056/NEJMoa022436>.
- [49] Reginster JY, Seeman E, De Vernejoul MC, Adami S, Compston J, Phenekos C, *et al.* Strontium ranelate reduces the risk of non-vertebral fractures in postmenopausal women with osteoporosis: Treatment of Peripheral Osteoporosis (TROPOS) study. *The Journal of Clinical Endocrinology and Metabolism*. 2005; 90: 2816–2822. <https://doi.org/10.1210/jc.2004-1774>.
- [50] Marx D, Rahimnejad Yazdi A, Papini M, Towler M. A review of the latest insights into the mechanism of action of strontium in bone. *Bone Reports*. 2020; 12: 100273. <https://doi.org/10.1016/j.bonr.2020.100273>.
- [51] Takaoka S, Yamaguchi T, Yano S, Yamauchi M, Sugimoto T. The Calcium-sensing Receptor (CaR) is involved in strontium ranelate-induced osteoblast differentiation and mineralization. *Hormone and Metabolic Research*. 2010; 42: 627–631. <https://doi.org/10.1055/s-0030-1255091>.
- [52] Sila-Asna M, Bunyaratvej A, Maeda S, Kitaguchi H, Bunyaratvej N. Osteoblast differentiation and bone formation gene expression in strontium-inducing bone marrow mesenchymal stem cell. *The Kobe Journal of Medical Sciences*. 2007; 53: 25–35.
- [53] Mizumachi H, Yoshida S, Tomokiyo A, Hasegawa D, Hamano S, Yuda A, *et al.* Calcium-sensing receptor-ERK signaling promotes odontoblastic differentiation of human dental pulp cells. *Bone*. 2017; 101: 191–201. <https://doi.org/10.1016/j.bone.2017.05.012>.
- [54] Pan FY, Li ZM, Liu XW, Luo Y, Ma Z, Feng SX, *et al.* Effect of strontium ranelate on rabbits with steroid-induced osteonecrosis of femoral head through TGF-  1/BMP2 pathway. *European Review for Medical and Pharmacological Sciences*. 2020; 24: 1000–1006. https://doi.org/10.26355/eurev_202002_20150.
- [55] Quade M, Vater C, Schlootz S, Bolte J, Langanke R, Bretschneider H, *et al.* Strontium enhances BMP-2 mediated bone regeneration in a femoral murine bone defect model. *Journal of Biomedical Materials Research. Part B, Applied Biomaterials*. 2020; 108: 174–182. <https://doi.org/10.1002/jbm.b.34376>.
- [56] Yu H, Liu Y, Yang X, He J, Zhang F, Zhong Q, *et al.* Strontium ranelate promotes chondrogenesis through inhibition of the Wnt/  -catenin pathway. *Stem Cell Research & Therapy*. 2021; 12: 296. <https://doi.org/10.1186/s13287-021-02372-z>.
- [57] Li Y, Yue J, Liu Y, Wu J, Guan M, Chen D, *et al.* Strontium regulates stem cell fate during osteogenic differentiation through asymmetric cell division. *Acta Biomaterialia*. 2021; 119: 432–

443. <https://doi.org/10.1016/j.actbio.2020.10.030>.
- [58] Yang F, Yang D, Tu J, Zheng Q, Cai L, Wang L. Strontium enhances osteogenic differentiation of mesenchymal stem cells and in vivo bone formation by activating Wnt/ctenin signaling. *Stem Cells*. 2011; 29: 981–991. <https://doi.org/10.1002/stem.646>.
- [59] Zhang X, Cui J, Cheng L, Lin K. Enhancement of osteoporotic bone regeneration by strontium-substituted 45S5 bioglass via time-dependent modulation of autophagy and the Akt/mTOR signaling pathway. *Journal of Materials Chemistry. B*. 2021; 9: 3489–3501. <https://doi.org/10.1039/d0tb02991b>.
- [60] Cheng Y, Huang L, Wang Y, Huo Q, Shao Y, Bao H, *et al*. Strontium promotes osteogenic differentiation by activating autophagy via the AMPK/mTOR signaling pathway in MC3T3 E1 cells. *International Journal of Molecular Medicine*. 2019; 44: 652–660. <https://doi.org/10.3892/ijmm.2019.4216>.
- [61] Saidak Z, Marie PJ. Strontium signaling: molecular mechanisms and therapeutic implications in osteoporosis. *Pharmacology & Therapeutics*. 2012; 136: 216–226. <https://doi.org/10.1016/j.pharmthera.2012.07.009>.
- [62] Wen X, Hu G, Xiao X, Zhang X, Zhang Q, Guo H, *et al*. FGF2 positively regulates osteoclastogenesis via activating the ERK-CREB pathway. *Archives of Biochemistry and Biophysics*. 2022; 727: 109348. <https://doi.org/10.1016/j.abb.2022.109348>.
- [63] Xie Y, Bao Z, Wang Z, Du D, Chen G, Liu C, *et al*. Magnesium Ascorbyl Phosphate Promotes Bone Formation Via CaMKII Signaling. *Journal of Bone and Mineral Research*. 2023; 38: 1015–1031. <https://doi.org/10.1002/jbmr.4820>.
- [64] Boyce BF, Xing L. Functions of RANKL/RANK/OPG in bone modeling and remodeling. *Archives of Biochemistry and Biophysics*. 2008; 473: 139–146. <https://doi.org/10.1016/j.abb.2008.03.018>.
- [65] Baron R, Tsouderos Y. In vitro effects of S12911-2 on osteoclast function and bone marrow macrophage differentiation. *European Journal of Pharmacology*. 2002; 450: 11–17. [https://doi.org/10.1016/s0014-2999\(02\)02040-x](https://doi.org/10.1016/s0014-2999(02)02040-x).
- [66] Caudrillier A, Hurtel-Lemaire AS, Wattel A, Cournarie F, Godin C, Petit L, *et al*. Strontium ranelate decreases receptor activator of nuclear factor- κ B ligand-induced osteoclastic differentiation in vitro: involvement of the calcium-sensing receptor. *Molecular Pharmacology*. 2010; 78: 569–576. <https://doi.org/10.1124/mol.109.063347>.
- [67] Dotta TC, Hayann L, de Padua Andrade Almeida L, Nogueira LFB, Arnez MM, Castelo R, *et al*. Strontium Carbonate and Strontium-Substituted Calcium Carbonate Nanoparticles Form Protective Deposits on Dentin Surface and Enhance Human Dental Pulp Stem Cells Mineralization. *Journal of Functional Biomaterials*. 2022; 13: 250. <https://doi.org/10.3390/jfb13040250>.
- [68] Hayann L, da Rocha VF, Cândido MF, Vicente RM, Andrilli LHS, Fukada SY, *et al*. A nontoxic strontium nanoparticle that holds the potential to act upon osteocompetent cells: An in vitro and in vivo characterization. *Journal of Biomedical Materials Research. Part A*. 2024; 112: 1518–1531. <https://doi.org/10.1002/jbm.a.37708>.
- [69] Cruz MAE, Tovani CB, Favarin BZ, Soares MPR, Fukada SY, Ciancaglini P, *et al*. Synthesis of Sr-morin complex and its in vitro response: decrease in osteoclast differentiation while sustaining osteoblast mineralization ability. *Journal of Materials Chemistry. B*. 2019; 7: 823–829. <https://doi.org/10.1039/c8tb02045k>.
- [70] Li S, He Y, Li J, Sheng J, Long S, Li Z, *et al*. Titanium scaffold loaded with strontium and copper double-doped hydroxyapatite can inhibit bacterial growth and enhance osteogenesis. *Journal of Biomaterials Applications*. 2022; 37: 195–203. <https://doi.org/10.1177/08853282221080525>.
- [71] López-Valverde N, Muriel-Fernández J, Gómez de Diego R, Ramírez JM, López-Valverde A. Effect of Strontium-Coated Titanium Implants on Osseointegration in Animal Models: A Literature Systematic Review. *The International Journal of Oral & Maxillofacial Implants*. 2019; 34: 1389–1396. <https://doi.org/10.11607/jomi.7827>.
- [72] Prabha RD, Nair BP, Ditzel N, Kjemis J, Nair PD, Kassem M. Strontium functionalized scaffold for bone tissue engineering. *Materials Science & Engineering. C, Materials for Biological Applications*. 2019; 94: 509–515. <https://doi.org/10.1016/j.msec.2018.09.054>.
- [73] Prabha RD, Ding M, Bollen P, Ditzel N, Varma HK, Nair PD, *et al*. Strontium ion reinforced bioceramic scaffold for load bearing bone regeneration. *Materials Science & Engineering. C, Materials for Biological Applications*. 2020; 109: 110427. <https://doi.org/10.1016/j.msec.2019.110427>.
- [74] Priam F, Ronco V, Locker M, Bourd K, Bonnefoix M, Duchêne T, *et al*. New cellular models for tracking the odontoblast phenotype. *Archives of Oral Biology*. 2005; 50: 271–277. <https://doi.org/10.1016/j.archoralbio.2004.10.007>.
- [75] Lacerda-Pinheiro S, Dimitrova-Nakov S, Harichane Y, Souyri M, Petit-Cocault L, Legrès L, *et al*. Concomitant multipotent and unipotent dental pulp progenitors and their respective contribution to mineralised tissue formation. *European Cells & Materials*. 2012; 23: 371–386. <https://doi.org/10.22203/ecm.v023a29>.
- [76] Mosmann T. Rapid colorimetric assay for cellular growth and survival: application to proliferation and cytotoxicity assays. *Journal of Immunological Methods*. 1983; 65: 55–63. [https://doi.org/10.1016/0022-1759\(83\)90303-4](https://doi.org/10.1016/0022-1759(83)90303-4).
- [77] Kirsch T, Nah HD, Shapiro IM, Pacifici M. Regulated production of mineralization-competent matrix vesicles in hypertrophic chondrocytes. *The Journal of Cell Biology*. 1997; 137: 1149–1160. <https://doi.org/10.1083/jcb.137.5.1149>.
- [78] Chaudhary SC, Kuzynski M, Bottini M, Beniash E, Dokland T, Mobley CG, *et al*. Phosphate induces formation of matrix vesicles during odontoblast-initiated mineralization in vitro. *Matrix Biology*. 2016; 52–54: 284–300. <https://doi.org/10.1016/j.matbio.2016.02.003>.
- [79] Favarin BZ, Bolean M, Ramos AP, Magrini A, Rosato N, Millán JL, *et al*. Lipid composition modulates ATP hydrolysis and calcium phosphate mineral propagation by TNAP-harboring proteoliposomes. *Archives of Biochemistry and Biophysics*. 2020; 691: 108482. <https://doi.org/10.1016/j.abb.2020.108482>.
- [80] Genge BR, Wu LNY, Wuthier RE. Kinetic analysis of mineral formation during in vitro modeling of matrix vesicle mineralization: effect of annexin A5, phosphatidylserine, and type II collagen. *Analytical Biochemistry*. 2007; 367: 159–166. <https://doi.org/10.1016/j.ab.2007.04.029>.
- [81] Vilela AFL, Patrício MR, Nobre-Azevedo P, de Carvalho JCS, Defelippo-Felippe TV, Pontes NNH, *et al*. Enhanced lipidomics workflows for plasma and extracellular vesicles through advanced liquid chromatography-tandem mass spectrometry integrated. *Talanta*. 2025; 291: 127847. <https://doi.org/10.1016/j.talanta.2025.127847>.
- [82] Kuzynski M, Goss M, Bottini M, Yadav MC, Mobley C, Winters T, *et al*. Dual role of the Trps1 transcription factor in dentin mineralization. *The Journal of Biological Chemistry*. 2014; 289: 27481–27493. <https://doi.org/10.1074/jbc.M114.550129>.
- [83] Bai M, Chen H, Zhang Z, Liu X, Zhang D, Wang C. Substrate stiffness promotes dentinogenesis via LAMB1-FAK-MEK1/2 signaling axis. *Oral Diseases*. 2024; 30: 562–574. <https://doi.org/10.1111/odi.14469>.
- [84] Yu F, Huo F, Li F, Zuo Y, Wang C, Ye L. Aberrant NF- κ B activation in odontoblasts orchestrates inflammatory matrix degradation and mineral resorption. *International Journal of Oral Science*. 2022; 14: 6. <https://doi.org/10.1038/>

s41368-022-00159-3.

- [85] Miranda TS, Napimoga MH, De Franco L, Marins LM, Malta FDS, Pontes LA, *et al.* Strontium ranelate improves alveolar bone healing in estrogen-deficient rats. *Journal of Periodontology*. 2020; 91: 1465–1474. <https://doi.org/10.1002/JPER.19-0561>.
- [86] Marie PJ. Strontium ranelate: a physiological approach for optimizing bone formation and resorption. *Bone*. 2006; 38: S10–S14. <https://doi.org/10.1016/j.bone.2005.07.029>.
- [87] Marie PJ. Strontium ranelate: a novel mode of action optimizing bone formation and resorption. *Osteoporosis International*. 2005; 16: S7–S10. <https://doi.org/10.1007/s00198-004-1753-8>.
- [88] Deeks ED, Dhillon S. Strontium ranelate: a review of its use in the treatment of postmenopausal osteoporosis. *Drugs*. 2010; 70: 733–759. <https://doi.org/10.2165/10481900-000000000-00000>.
- [89] Reginster JY. Strontium ranelate in osteoporosis. *Current Pharmaceutical Design*. 2002; 8: 1907–1916. <https://doi.org/10.2174/1381612023393639>.
- [90] Couce ML, Saenz de Pipaon M. Bone Mineralization and Calcium Phosphorus Metabolism. *Nutrients*. 2021; 13: 3692. <https://doi.org/10.3390/nu13113692>.
- [91] Murshed M. Mechanism of Bone Mineralization. *Cold Spring Harbor Perspectives in Medicine*. 2018; 8: a031229. <https://doi.org/10.1101/cshperspect.a031229>.
- [92] Schneider MR. Von Kossa and his staining technique. *Histochemistry and Cell Biology*. 2021; 156: 523–526. <https://doi.org/10.1007/s00418-021-02051-3>.
- [93] Webb JCJ, Spencer RF. The role of polymethylmethacrylate bone cement in modern orthopaedic surgery. *The Journal of Bone and Joint Surgery. British Volume*. 2007; 89: 851–857. <https://doi.org/10.1302/0301-620X.89B7.19148>.
- [94] Campana V, Milano G, Pagano E, Barba M, Cicione C, Salonna G, *et al.* Bone substitutes in orthopaedic surgery: from basic science to clinical practice. *Journal of Materials Science. Materials in Medicine*. 2014; 25: 2445–2461. <https://doi.org/10.1007/s10856-014-5240-2>.
- [95] Darjanki CM, Hananta JS, Prahasanti C, Ulfah N, Kusumawardani B, Wijaksana IKE, *et al.* Expression of VEGF and BMP-2 in Osteoblast cells exposed to a combination of polymethylmethacrylate (PMMA) and hydroxyapatite (HAP). *Journal of Oral Biology and Craniofacial Research*. 2023; 13: 243–248. <https://doi.org/10.1016/j.jobcr.2023.02.006>.
- [96] Liu Z, Tang Y, Kang T, Rao M, Li K, Wang Q, *et al.* Synergistic effect of HA and BMP-2 mimicking peptide on the bioactivity of HA/PMMA bone cement. *Colloids and Surfaces. B, Biointerfaces*. 2015; 131: 39–46. <https://doi.org/10.1016/j.colsurfb.2015.04.032>.
- [97] Goldberg M, Kulkarni AB, Young M, Boskey A. Dentin: structure, composition and mineralization. *Frontiers in Bioscience (Elite Edition)*. 2011; 3: 711–735. <https://doi.org/10.2741/e281>.
- [98] Dzumukova M, Brunner TM, Miotla-Zarebska J, Heinrich F, Brylka L, Mashregi MF, *et al.* Mechanical forces couple bone matrix mineralization with inhibition of angiogenesis to limit adolescent bone growth. *Nature Communications*. 2022; 13: 3059. <https://doi.org/10.1038/s41467-022-30618-8>.
- [99] Bakhshian Nik A, Hutcheson JD, Aikawa E. Extracellular Vesicles As Mediators of Cardiovascular Calcification. *Frontiers in Cardiovascular Medicine*. 2017; 4: 78. <https://doi.org/10.3389/fcvm.2017.00078>.
- [100] van Leeuwen JP, van Driel M, van den Bermd GJ, Pols HA. Vitamin D control of osteoblast function and bone extracellular matrix mineralization. *Critical Reviews in Eukaryotic Gene Expression*. 2001; 11: 199–226.
- [101] Park H, Jo S, Jang MA, Choi SH, Kim TH. Dkkopf-1 promotes matrix mineralization of osteoblasts by regulating Ca²⁺-CAMK2A- CREB1 pathway. *BMB Reports*. 2022; 55: 627–632. <https://doi.org/10.5483/BMBRep.2022.55.12.103>.
- [102] Hadi T, Barrichon M, Mourtialon P, Wendremaire M, Garrido C, Sagot P, *et al.* Biphasic Erk1/2 activation sequentially involving Gs and Gi signaling is required in beta3-adrenergic receptor-induced primary smooth muscle cell proliferation. *Biochimica et Biophysica Acta*. 2013; 1833: 1041–1051. <https://doi.org/10.1016/j.bbamcr.2013.01.019>.
- [103] Matsubayashi Y, Ebisuya M, Honjoh S, Nishida E. ERK activation propagates in epithelial cell sheets and regulates their migration during wound healing. *Current Biology*. 2004; 14: 731–735. <https://doi.org/10.1016/j.cub.2004.03.060>.
- [104] Steven A, Friedrich M, Jank P, Heimer N, Budczies J, Denkert C, *et al.* What turns CREB on? And off? And why does it matter? *Cellular and Molecular Life Sciences*. 2020; 77: 4049–4067. <https://doi.org/10.1007/s00018-020-03525-8>.
- [105] Sapio L, Salzillo A, Ragone A, Illiano M, Spina A, Naviglio S. Targeting CREB in Cancer Therapy: A Key Candidate or One of Many? An Update. *Cancers*. 2020; 12: 3166. <https://doi.org/10.3390/cancers12113166>.
- [106] Zhang H, Yang S, Wang J, Jiang Y. Blockade of AMPK-Mediated cAMP-PKA-CREB/ATF1 Signaling Synergizes with Aspirin to Inhibit Hepatocellular Carcinoma. *Cancers*. 2021; 13: 1738. <https://doi.org/10.3390/cancers13071738>.
- [107] Mantamadiotis T, Papalexis N, Dworkin S. CREB signalling in neural stem/progenitor cells: recent developments and the implications for brain tumour biology. *BioEssays*. 2012; 34: 293–300. <https://doi.org/10.1002/bies.201100133>.
- [108] Sun P, He L, Jia K, Yue Z, Li S, Jin Y, *et al.* Regulation of body length and bone mass by Gpr126/Adgrg6. *Science Advances*. 2020; 6: eaaz0368. <https://doi.org/10.1126/sciadv.aaz0368>.
- [109] Matsumoto T, Kuriwaka-Kido R, Kondo T, Endo I, Kido S. Regulation of osteoblast differentiation by interleukin-11 via AP-1 and Smad signaling. *Endocrine Journal*. 2012; 59: 91–101. <https://doi.org/10.1507/endocrj.ej11-0219>.
- [110] Huang S, Ren Y, Wang P, Li Y, Wang X, Zhuang H, *et al.* Transcription factor CREB is involved in CaSR-mediated cytoskeleton gene expression. *Anatomical Record*. 2015; 298: 501–512. <https://doi.org/10.1002/ar.23089>.
- [111] Avlani VA, Ma W, Mun HC, Leach K, Delbridge L, Christopoulos A, *et al.* Calcium-sensing receptor-dependent activation of CREB phosphorylation in HEK293 cells and human parathyroid cells. *American Journal of Physiology. Endocrinology and Metabolism*. 2013; 304: E1097–E1104. <https://doi.org/10.1152/ajpendo.00054.2013>.
- [112] McNeil SE, Hobson SA, Nipper V, Rodland KD. Functional calcium-sensing receptors in rat fibroblasts are required for activation of SRC kinase and mitogen-activated protein kinase in response to extracellular calcium. *The Journal of Biological Chemistry*. 1998; 273: 1114–1120. <https://doi.org/10.1074/jbc.273.2.1114>.
- [113] Aimaiti A, Maimaitiyiming A, Boyong X, Aji K, Li C, Cui L. Low-dose strontium stimulates osteogenesis but high-dose doses cause apoptosis in human adipose-derived stem cells via regulation of the ERK1/2 signaling pathway. *Stem Cell Research & Therapy*. 2017; 8: 282. <https://doi.org/10.1186/s13287-017-0726-8>.
- [114] Zhang X, Li H, Lin C, Ning C, Lin K. Synergetic topography and chemistry cues guiding osteogenic differentiation in bone marrow stromal cells through ERK1/2 and p38 MAPK signaling pathway. *Biomaterials Science*. 2018; 6: 418–430. <https://doi.org/10.1039/c7bm01044c>.
- [115] Li L, Wang Y, Wang Z, Xue D, Dai C, Gao X, *et al.* Knockdown of FOXA1 enhances the osteogenic differentiation of human bone marrow mesenchymal stem cells partly via activation of the ERK1/2 signalling pathway. *Stem Cell Research & Therapy*. 2022; 13: 456. <https://doi.org/10.1186/s13287-022-03133-2>.

- [116] Jiang Y, Xin N, Xiong Y, Guo Y, Yuan Y, Zhang Q, *et al.* α CGRP Regulates Osteogenic Differentiation of Bone Marrow Mesenchymal Stem Cells Through ERK1/2 and p38 MAPK Signaling Pathways. *Cell Transplantation*. 2022; 31: 9636897221107636. <https://doi.org/10.1177/09636897221107636>.
- [117] Bechhoff G, Radisson J, Bessueille L, Bouchekioua-Bouzaghoul K, Buchet R. Distinct actions of strontium on mineral formation in matrix vesicles. *Biochemical and Biophysical Research Communications*. 2008; 373: 378–381. <https://doi.org/10.1016/j.bbrc.2008.06.044>.
- [118] Simão AMS, Beloti MM, Cezarino RM, Rosa AL, Pizauro JM, Ciancaglini P. Membrane-bound alkaline phosphatase from ectopic mineralization and rat bone marrow cell culture. *Comparative Biochemistry and Physiology. Part A, Molecular & Integrative Physiology*. 2007; 146: 679–687. <https://doi.org/10.1016/j.cbpa.2006.05.008>.
- [119] Millán JL. Alkaline Phosphatases: Structure, substrate specificity and functional relatedness to other members of a large superfamily of enzymes. *Purinergic Signalling*. 2006; 2: 335–341. <https://doi.org/10.1007/s11302-005-5435-6>.
- [120] Millán JL, Whyte MP. Alkaline Phosphatase and Hypophosphatasia. *Calcified Tissue International*. 2016; 98: 398–416. <https://doi.org/10.1007/s00223-015-0079-1>.
- [121] Wuthier RE, Chin JE, Hale JE, Register TC, Hale LV, Ishikawa Y. Isolation and characterization of calcium-accumulating matrix vesicles from chondrocytes of chicken epiphyseal growth plate cartilage in primary culture. *The Journal of Biological Chemistry*. 1985; 260: 15972–15979.
- [122] Ferreira CR, Cruz MAE, Bolean M, Andrioli LHDS, Millán JL, Ramos AP, *et al.* Annexin A5 stabilizes matrix vesicle-biomimetic lipid membranes: unravelling a new role of annexins in calcification. *European Biophysics Journal*. 2023; 52: 721–733. <https://doi.org/10.1007/s00249-023-01687-4>.
- [123] Ciancaglini P, Simão AMS, Camolezi FL, Millán JL, Pizauro JM. Contribution of matrix vesicles and alkaline phosphatase to ectopic bone formation. *Brazilian Journal of Medical and Biological Research*. 2006; 39: 603–610. <https://doi.org/10.1590/s0100-879x2006000500006>.
- [124] Bolean M, Izzi B, van Kerckhoven S, Bottini M, Ramos AP, Millán JL, *et al.* Matrix vesicle biomimetics harboring Annexin A5 and alkaline phosphatase bind to the native collagen matrix produced by mineralizing vascular smooth muscle cells. *Biochimica et Biophysica Acta. General Subjects*. 2020; 1864: 129629. <https://doi.org/10.1016/j.bbagen.2020.129629>.
- [125] Zhang J, Zeng W, Han Y, Lee WR, Liou J, Jiang Y. Lysosomal LAMP proteins regulate lysosomal pH by direct inhibition of the TMEM175 channel. *Molecular Cell*. 2023; 83: 2524–2539.e7. <https://doi.org/10.1016/j.molcel.2023.06.004>.
- [126] Blair HC, Larrouture QC, Tourkova IL, Liu L, Bian JH, Stolz DB, *et al.* Support of bone mineral deposition by regulation of pH. *American Journal of Physiology. Cell Physiology*. 2018; 315: C587–C597. <https://doi.org/10.1152/ajpcell.00056.2018>.
- [127] Rouso I, Deshpande A. Applications of Atomic Force Microscopy in HIV-1 Research. *Viruses*. 2022; 14: 648. <https://doi.org/10.3390/v14030648>.
- [128] Sebinelli HG, Andrioli LHS, Favarin BZ, Cruz MAE, Bolean M, Fiore M, *et al.* Shedding Light on the Role of Na,K-ATPase as a Phosphatase during Matrix-Vesicle-Mediated Mineralization. *International Journal of Molecular Sciences*. 2022; 23: 15072. <https://doi.org/10.3390/ijms232315072>.
- [129] Plaut JS, Strzelecka-Kiliszek A, Bozycki L, Pikula S, Buchet R, Mebarek S, *et al.* Quantitative atomic force microscopy provides new insight into matrix vesicle mineralization. *Archives of Biochemistry and Biophysics*. 2019; 667: 14–21. <https://doi.org/10.1016/j.abb.2019.04.003>.
- [130] Bolean M, Borin IA, Simão AMS, Bottini M, Bagatolli LA, Hoylaerts MF, *et al.* Topographic analysis by atomic force microscopy of proteoliposomes matrix vesicle mimetics harboring TNAP and AnxA5. *Biochimica et Biophysica Acta. Biomembranes*. 2017; 1859: 1911–1920. <https://doi.org/10.1016/j.bbame.2017.05.010>.
- [131] Airola MV, Hannun YA. Sphingolipid metabolism and neutral sphingomyelinases. *Handbook of Experimental Pharmacology*. 2013; 57–76. https://doi.org/10.1007/978-3-7091-1368-4_3.
- [132] Ermonval M, Baychelier F, Fonta C. TNAP, an Essential Player in Membrane Lipid Rafts of Neuronal Cells. *Subcellular Biochemistry*. 2015; 76: 167–183. https://doi.org/10.1007/978-94-017-7197-9_9.
- [133] Garcia AF, Simão AMS, Bolean M, Hoylaerts MF, Millán JL, Ciancaglini P, *et al.* Effects of GPI-anchored TNAP on the dynamic structure of model membranes. *Physical Chemistry Chemical Physics*. 2015; 17: 26295–26301. <https://doi.org/10.1039/c5cp02377g>.
- [134] Ciancaglini P, Yadav MC, Simão AMS, Narisawa S, Pizauro JM, Farquharson C, *et al.* Kinetic analysis of substrate utilization by native and TNAP-, NPPI-, or PHOSPHO1-deficient matrix vesicles. *Journal of Bone and Mineral Research*. 2010; 25: 716–723. <https://doi.org/10.1359/jbmr.091023>.
- [135] Bolean M, Simão AMS, Favarin BZ, Millán JL, Ciancaglini P. The effect of cholesterol on the reconstitution of alkaline phosphatase into liposomes. *Biophysical Chemistry*. 2010; 152: 74–79. <https://doi.org/10.1016/j.bpc.2010.08.002>.
- [136] Almeida PF, Carter FE, Kilgour KM, Raymonda MH, Tejada E. Heat Capacity of DPPC/Cholesterol Mixtures: Comparison of Single Bilayers with Multibilayers and Simulations. *Langmuir*. 2018; 34: 9798–9809. <https://doi.org/10.1021/acs.langmuir.8b01774>.
- [137] Barenholz Y. Cholesterol and other membrane active sterols: from membrane evolution to “rafts”. *Progress in Lipid Research*. 2002; 41: 1–5. [https://doi.org/10.1016/s0163-7827\(01\)00016-9](https://doi.org/10.1016/s0163-7827(01)00016-9).
- [138] Simons K, Ikonen E. Functional rafts in cell membranes. *Nature*. 1997; 387: 569–572. <https://doi.org/10.1038/42408>.
- [139] During A, Penel G, Hardouin P. Understanding the local actions of lipids in bone physiology. *Progress in Lipid Research*. 2015; 59: 126–146. <https://doi.org/10.1016/j.plipres.2015.06.002>.
- [140] During A, Coutel X, Bertheaume N, Penel G, Olejnik C. Long Term Ovariectomy-Induced Osteoporosis is Associated with High Stearoyl-CoA Desaturase Indexes in Rat Femur. *Calcified Tissue International*. 2020; 106: 315–324. <https://doi.org/10.1007/s00223-019-00637-7>.
- [141] Ogretmen B. Sphingolipid metabolism in cancer signalling and therapy. *Nature Reviews. Cancer*. 2018; 18: 33–50. <https://doi.org/10.1038/nrc.2017.96>.
- [142] Aubin I, Adams CP, Opsahl S, Septier D, Bishop CE, Auge N, *et al.* A deletion in the gene encoding sphingomyelin phosphodiesterase 3 (Smpd3) results in osteogenesis and dentinogenesis imperfecta in the mouse. *Nature Genetics*. 2005; 37: 803–805. <https://doi.org/10.1038/ng1603>.
- [143] Goldberg M, Opsahl S, Aubin I, Septier D, Chaussain-Miller C, Boskey A, *et al.* Sphingomyelin degradation is a key factor in dentin and bone mineralization: lessons from the fro/fro mouse. The chemistry and histochemistry of dentin lipids. *Journal of Dental Research*. 2008; 87: 9–13. <https://doi.org/10.1177/154405910808700103>.
- [144] Khavandgar Z, Alebrahim S, Eimar H, Tamimi F, McKee MD, Murshed M. Local regulation of tooth mineralization by sphingomyelin phosphodiesterase 3. *Journal of Dental Research*. 2013; 92: 358–364. <https://doi.org/10.1177/0022034513478429>.